Front. Chem. Sci. Eng. 2024, 18(7): 79
https://doi.org/10.1007/s11705-024-2434-0

REVIEW ARTICLE

Single-atom catalysis: a promising avenue for precisely controlling reaction pathways

Xiaobo Yang, Xuning Li (✉), Yanqiang Huang (✉)

State Key Laboratory of Catalysis, Dalian Institute of Chemical Physics, Chinese Academy of Sciences, Dalian 116023, China

Abstract Single-atom catalysts (SACs), characterized by exceptionally high atom efficiency, have garnered significant attention across various catalytic reactions. Recent studies have showcased SACs with robust capabilities for precise catalysis, specifically targeting reactions along designated pathways. This review focuses on the advances in the precise activation and reconstruction of chemical bonds on SACs, including precise activation of C–O and C–H bonds and selective couplings involving C–C and C–N bonds. Our discussion begins with a thorough exploration of the factors that render SACs skilled in precise catalytic processes, encompassing the narrow *d*-band electronic state of single atom site resulting in the adsorption tendency, isolate site resulting in unique adsorption structure, and synergy effect of a single atom site with its neighbors. Subsequently, we elaborate on the applications of SACs in electrocatalysis and thermocatalysis including four prominent reactions, namely, electrochemical CO_2 reduction, urea electrochemical synthesis, CO_2 hydrogenation, and CH_4 activation. Then the concept of rational design of SACs for precisely controlling reaction pathways is discussed from the aspects of pore structure design, support-metal strong interaction, and support hydrophilic/hydrophobic. Finally, we summarize the challenges encountered by SACs in the field of precise catalytic processes and outline prospects for their further development in this domain.

Keywords single atom catalysts, selective oxidation, CO_2RR, bond coupling

1 Introduction

Over the past few decades, rapid economic development has been facilitated by advancements in catalytic techniques [1−4]. For instance, the synthesis of NH_3 from N_2 and H_2 revolutionized urea industrial production and boosted grain output [5−7]. Fischer-Tropsch synthesis from CO and H_2 to high-value-added chemicals [8−10]. Electrode materials development promotes the large-scaling application of Li-ion batteries in electricity cars [11−15]. Looking ahead, catalysis will continue to play a pivotal role in addressing environmental and energy challenges. This includes converting CO_2 [16−19] and N_2 [20−22] into valuable chemicals through electric energy, transforming liquid fuel into electric energy in fuel cells [23,24], synthesizing high-value chemicals using thermo or photo energy [25], biomass conversion [26−28], and more. In various complex catalytic systems, the performance of catalyst significantly influences the efficiency of the catalytic process, determining reaction activity, selectivity, and stability [4,29−32] (Fig. 1).

Increasing the number of active sites and enhancing intrinsic activity are both crucial in the catalyst design and synthesis. The activity number is influenced by the structure of the catalyst and the distribution of active sites. In this aspect, nanowires [33,34], nanosheets [35], and core-shell structure catalysts [36] are designed to improve the number of active sites. On the other hand, intrinsic activity is affected by the electronic structure and adsorption nature of the active site. Following the Sabatier principle [37−39], excessively strong adsorption is harmful to intermediate desorption, while overly weak adsorption results in inadequate reactant activation. Hence, regulating the electronic structure of catalyst sites to control adsorption ability is a useful approach to enhance intrinsic activity. Based on these two-catalyst design rules, the concept of the single-atom catalyst (SAC) attracted much attention once it was put forward [40,41]. On one hand, it shows ultrahigh atom efficiency due to all metals being isolated activate sites. On the other hand, the electronic structure and the catalytic performance of the single atom site can be regulated by

Received December 22, 2023; accepted February 19, 2024;
online June 15, 2024

E-mails: lixn@dicp.ac.cn (Li X), yqhuang@dicp.ac.cn (Huang Y)

controlling its coordination environment [42]. Besides, the SAC always shows high reaction consistency and product selectivity due to its uniform catalyze site structure [42−45] (Fig. 2).

Real reaction condition is more complex because most chemical reactions go through multiple catalytic processes resulting in dispersive product distribution. For example, in the selectivity oxidation of CH_4 to value-added products, products can include CH_3OH, HCOOH, and CO_2 [46−48]. In electrochemical CO_2 reduction reaction (ECO_2RR), products may be CO, HCOOH, or various carbon compounds [49]. Ethanol can be oxidized

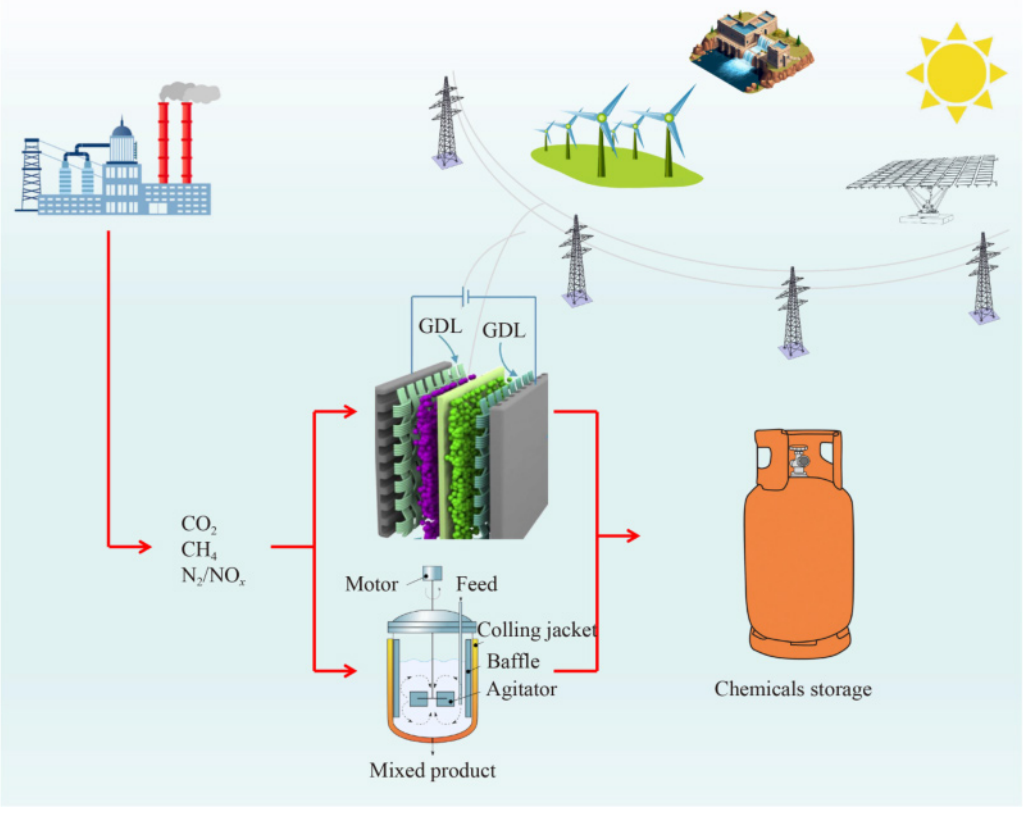

Fig. 1 The schematic of the importance of catalysis in current green synthesis.

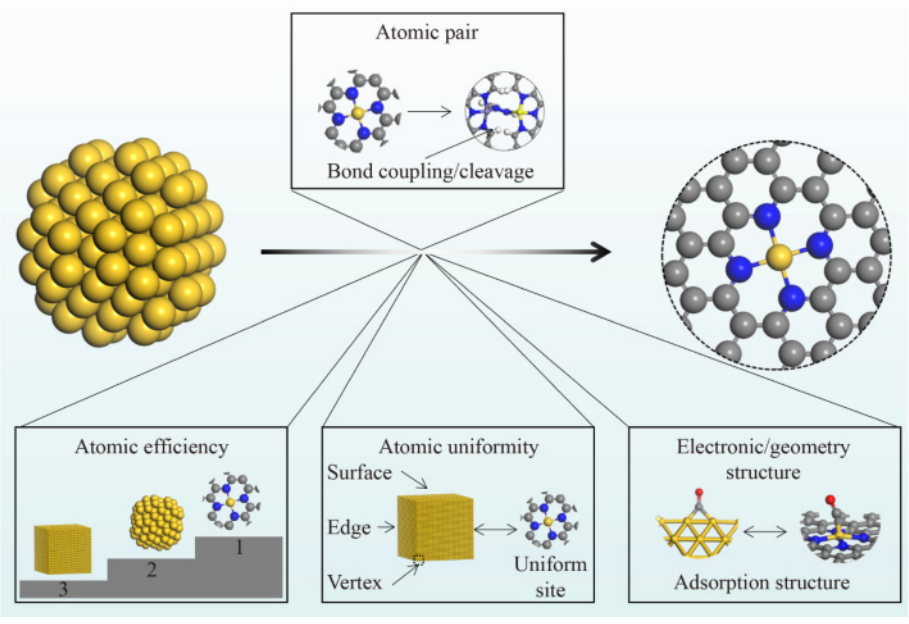

Fig. 2 The schematic of physicochemical property changes from nanocatalyst to single atom catalyst.

to CO_2 or CH_3COO^- in a fuel cell system [50,51]. Hence, precisely activating reactant molecules and controlling the catalytic process to achieve high selectivity of the product are crucial. Generally, these complex reaction processes can be classified into basic reaction steps, which include selective oxidation reaction, selective reduction reaction, bond cleavage, and bond coupling. Hence, achieving precise control over four fundamental steps enables specific reaction paths in reaction processes. Recently, many reports have shown that SACs can catalyze reactions with high selectivity or specific reaction paths, such as metal-nitrogen-carbon (M-NC) SACs with suitable coordination environment show ultra-high selectivity toward CO product during ECO_2RR [52], metal-oxide supported SAC can selective oxidation of CH_4 to CH_3OH with high selectivity [53,54]. Fe-based SAC with extremely high NH_3 product selectivity toward NO_3^- reduction [55]. Co-based SAC shows high efficiency in photo-catalysis CH_4 activation [56]. Co-based SAC can convert CO to CH_3OH products with high efficiency [57]. All these reports indicated that SAC is a potential candidate to precisely regulate reaction processes.

In this review, to illustrate the ability and advantage of SACs in precise operating reaction paths, and guide SACs design for specific reaction processes, we comprehensively discussed the basic mechanism and recent progress of precise catalytic reaction processes on SACs. The discussion starts with an in-depth exploration of the intrinsic reasons that SACs with precise activation capabilities, categorized into three critical points: (1) the narrow *d*-band electron state resulted in selectivity adsorption toward reactant and intermediates; (2) the isolate geometric site resulted in unique adsorption structure; (3) bond coupling and cleavage with the assistance of synergy effect. Subsequently, we outline the advancements of SACs in two important electrochemical synthesis reactions and two important thermocatalytic reactions: (1) CO_2 electrochemical reduction; (2) urea electrochemical synthesis; (3) CO_2 hydrogenation; (4) CH_4 activation. These reactions involve the activation of C–H bonds and C–O bonds, selective oxidation and reduction processes, as well as the coupling of C–C and C–N bonds. Then, we emphasized the importance of support and discussed the support design of SACs from the aspect of pore structure design and metal-support strong interaction. Besides, the influence of hydrophilic/hydrophobic of the support on catalytic performance and side reaction restrain was emphasized. Finally, we summarize the challenges in achieving precise activation processes using single-atom catalysis and propose future development directions. This review provides not only recent progress about the state of art design and applications of various reported SACs, but also recent achievements that have been well summarized, including the advantage of SACs in reaction path regulation, the mechanism understanding of SACs toward complex reactions, and support effect of SACs toward reaction path.

2 Why SACs is skilled in precise operating reaction path

In general, SACs exhibit excellent catalytic activity due to its ultra-high atom efficiency and high selectivity due to the uniform site structure [43,44,52]. More importantly, SACs catalyze reactions at isolated sites or individual atom pairs, demonstrating different catalytic properties compared to nanocatalysts due to their unique electronic and geometric structures [58]. Additionally, at times, SACs can catalyze complex reactions involving bond coupling or cleavage with the assistance of adjacent metal or nonmetal atoms. Based on the distinctions between SACs and nanocatalysts, the intrinsic reasons enabling SACs to achieve precise activation and control over reaction pathways can be summarized into three effects: (1) electronic effect: the distinctive electronic structure at the single site results in selective adsorption toward adsorbates; (2) geometric effect: isolate single site leads to different adsorption structures of adsorbates; (3) synergy effect: the synergy effect in SACs assists catalyzing and cleaving or coupling chemical bonds.

2.1 The electronic effect on SACs

For the SACs design, considering the atom efficiency achieves peak value, the most important two points are the activating reactant and regulation reaction path. Based on the Sabatier principle, the activation of reactant is affected by the adsorption nature of a single atom site. Besides, the selectivity of the catalyst relies on the uniformity of the active site and the selectivity adsorption ability toward some intermediate. The activation of the reactant molecule and the selectivity adsorption toward some intermediates are all affected by the electronic structure of the catalyst site. The electronic structure of SAC and nanocatalyst are quite different due to their different coordination environment, which makes SAC shows unique advantages in reactant activation and selectivity adsorption (Fig. 3(a)) [59]. Single metal site supported on N-doped carbon or metal oxidation coordinated with nonmetal atom (C/N/O) in general shows a narrow *d*-band electron structure, which is different from nanocatalyst with broad and continuous *d*-band electron structure (Fig. 3(a)) [59]. Based on the metal-adsorbate interaction relation that energy band with close energy level can interact stronger, the metal site with narrow *d*-band structure thus shows a strong tendency in selectivity adsorption, which is important in the regulation of reaction path (Fig. 3(b)) [60,61].

Besides, the narrow down of metal site *d*-band was also observed on SAA catalysts [61−63]. In SAA, even though the coordination environment of the single metal site is

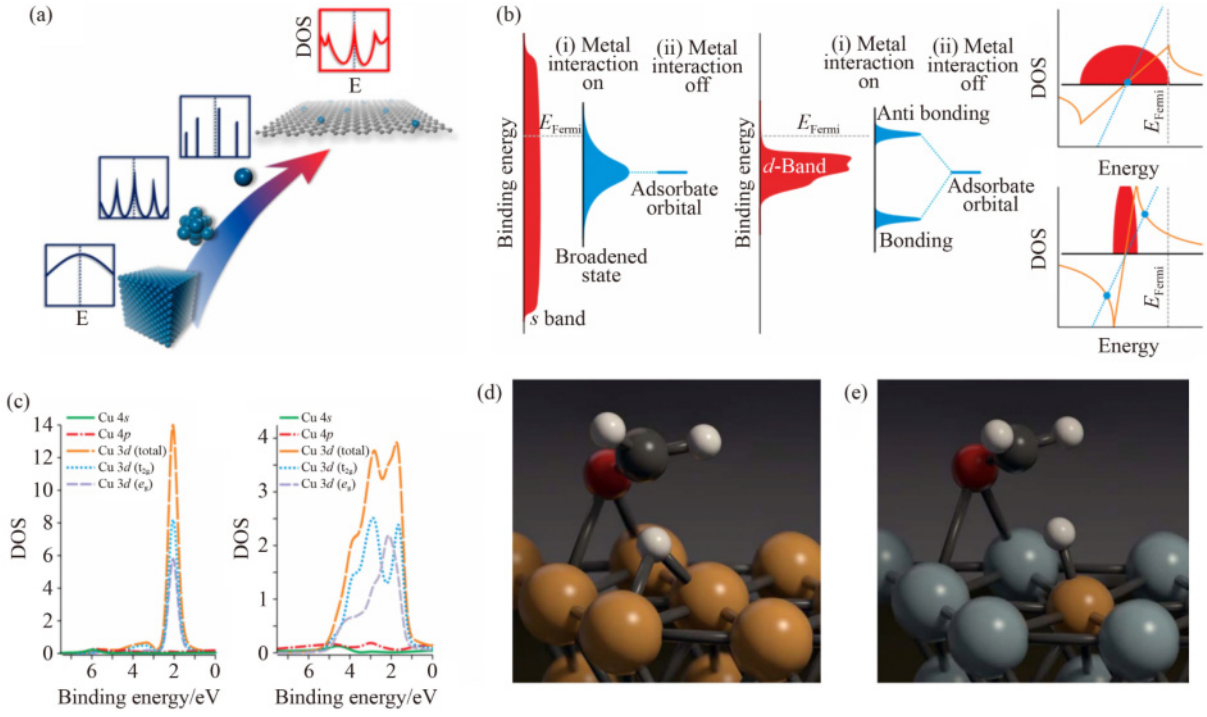

Fig. 3 (a) The electronic structure change from bulk catalyst to SAC. Reprinted with permission from Ref. [59], copyright 2019, American Chemical Society. (b) The interaction model between broad s and narrow d band of metal toward orbital of adsorbate, and a simplified interaction model of narrow/wide metal band orbital and molecular orbital of the adsorbate. (c) The calculated *d*-band structure of Cu atom on $AgCu_1$ SAA (single-atom alloy, left) and bulk Cu (right). (d, e) The schematic diagram of adsorbed structures of schizolytic CH_3O* on (d) Cu (111) and (e) $AgCu_1$ SAA (111) surface. Reprinted with permission from Ref. [61], copyright 2018, Springer Nature.

metal-metal coordination, which is similar to alloy or metal, the electronic structure of SAA is also different. For instance, in an $Ag_{31}Cu_1$ SAA, the d electron of the Cu atom is quite different to bulk Cu, and the *d*-band width of the Cu single site narrows down drastically, showing a "free atom-like" d electronic structure (Fig. 3(c)) [61]. The narrow *d*-band structure of the Cu atom shows different bonding modes with adsorbed O atom compared with bulk Cu. As for bulk Cu, the *d*-band is broad and continuous, it interacts with p_z orbital of the O atom to form a σ bonding orbital and a σ* antibonding orbital, while $Ag_{31}Cu_1$ with narrow Cu *d*-band both interacts with p_x, p_y, and p_z orbitals of the O atom and form σ/π bonding orbital and σ^*/π^* antibonding orbital, which increasing the binding strength of Cu–O bond significantly. Therefore, over $AgCu_1$ SAA surface, the H atom abstraction from CH_3O* is much easier than on Ag (111) due to the different adsorption structure of CH_2O-H* adsorption structure. (Figs. 3(d) and 3(e)) Such a narrow free-atom-like d-electron state is also observed on other MCu_1 SAAs, such as Pd, Pt, Ir [62,64]. Beneficial for the narrow *d*-band electron structure, the activation of reactant molecular is easier on SAA, such as the activation energy of H_2, NH_3, CH_4, CH_3OH on SAA surface is lower than on pure metal surface [64]. Except for the activation of reactant, the narrow *d*-band electron results in a tendency to adsorption in the different sites of an adsorbate molecule or different reactants. For instance, crotonaldehyde molecular is an important chemical raw material, in which both C=C and C=O double bonds exist (Fig. 4(a)) [63]. The regulation of the hydrogenation site to achieve high selectivity hydrogenation product is thus important. The key point of selectivity regulation of crotonaldehyde hydrogenation is the control of the adsorption site of C=C or C=O site on crotonaldehyde. On different SAA, the *d*-band center and the width of *d*-band electron are different. The single atom site with a narrow *d*-band shows stronger adsorption selectivity toward C=C and C=O bonds. Besides, based on the energy level close rule, when the *d*-band center of SAA is close to the Fermi level, it shows a higher tendency to adsorb the C=C bond (Fig. 4(b)). When the metal with a *d*-band center is far away Fermi level, however, it tends to adsorb C=O bonds. Further density of state analysis proved the antibonding orbital location of the C=O adsorption model on the $AuFe_1$ SAA surface and the C=C adsorption model on $AuPt_1$ SAA are over Fermi level (Fig. 4(c)), which contribution to the stabilize of adsorption system. The selectivity adsorption thus results in different product distribution on $AuFe_1$ and $AuPt_1$ SAAs.

In summary, the activity and selectivity of a catalyst are highly affected by its electron structure. The narrow *d*-band electron structure of SAC facilitates the activity and selectivity during process origin from the following two

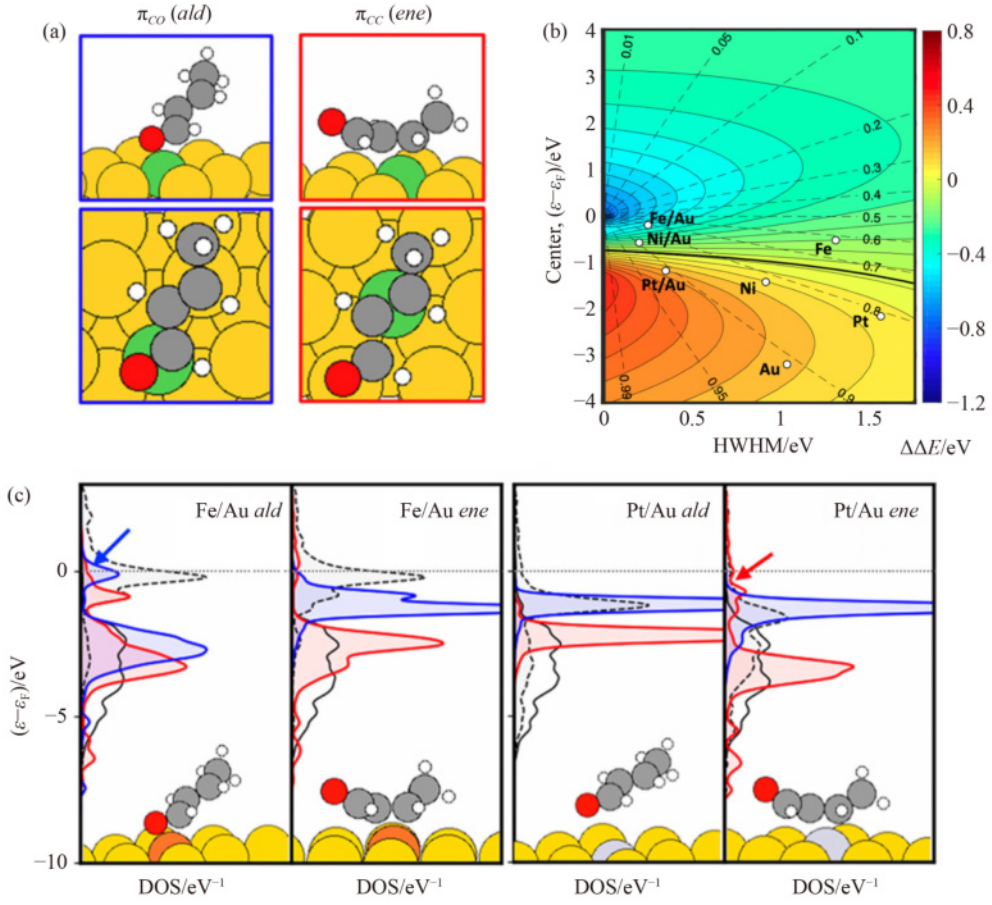

Fig. 4 (a) The schematic diagram of different structures (C=O species-left and C=C species-right) of crotonaldehyde adsorbed on SAA. (b) The adsorption tendency of crotonaldehyde on different SAAs and the differences in *d*-band interaction energy (*z*-axis) are affected by the *d*-band center value (*y*-axis) and width (HWHM, *x*-axis). (c) The density of state of crotonaldehyde adsorbed on $AuFe_1$ and $AuPt_1$ SAA with different adsorb models. Reprinted with permission from Ref. [63], copyright 2021, American Chemical Society.

aspects. (1) The narrow *d*-band electron promotes adsorption strength toward adsorbates thus promoting activation of reactant, such as activation of CH_4 on SAA is fast while not easy to be over oxidative. (2) The narrow *d*-band electron facilitates selectivity adsorption of the specific site of intermediates or reactant, the reaction path is thus operated and the reaction selectivity of the catalyst is thus increased.

2.2 The geometry effect on SACs

The reaction path is not only affected by the adsorption strength and tendency of intermediates but also affected by the adsorption structure of intermediates. Beneficial for the unique geometry structure, the adsorption states and structures of adsorbate are also different, which change the reaction path and product selectivity. Different from nanocatalysts that have a continuous metal site, SACs with an isolated metal site have special adsorption nature toward some reactants and intermediates, such as O_2, N_2, and CO molecules. For example, when the O_2 is adsorbed on continuous metal sites, it tends to be adsorbed on two metal sites and form two metal–O bonds, the O–O bond is stretched and thus easy to be cleavaged. However, when O_2 is adsorbed on a single atom site and two O atoms bond with one metal site, the cleavage of the O–O bond be difficult and thus need a higher energy barrier (Fig. 5(a)). In this aspect, the SAC is a potential candidate catalyst to regulate the reaction path of selective oxidation reaction. Yu et al. [65] reported a Pd single atom supported on TiO_2 with excellent reaction selectivity (more than 99%) toward oxygen hydrogenation to H_2O_2. Such a high selectivity is attributed to the huge energy barrier of O–O bond cleavage (1.89 eV) on the Pd_1/TiO_2, which is much larger than the O–O bond cleavage energy barrier (1.08 eV) on contrast Pd cluster (Pd_8O_8/TiO_2). The difference between Pd_1 single atom site and Pd_8O_8 cluster is attributed to the special geometry structure of Pd_1/TiO_2 (Fig. 5(b)). Similarly, when the single Co atom is supported on zeolites, it can activate O_2 and form a Co@Y-$O_2^{\delta-}$ structure as an electrophilic site to adsorb propylene. Therefore, the high selectivity of propylene oxide can be generated by Co@Y catalyst [66]. Qiao et al. [67]

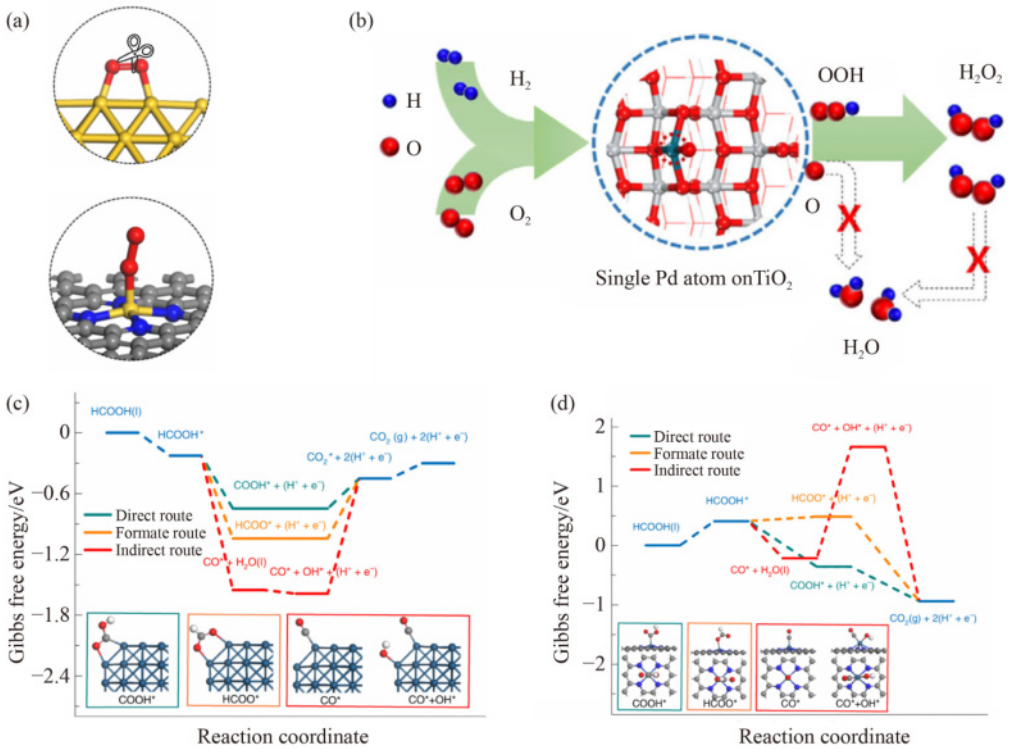

Fig. 5 (a) The schematic diagram of O_2 adsorbed on SAC and metal catalyst. (b) The schematic of H_2 oxidation on TiO_2 supported Pd single atom. Reprinted with permission from Ref. [65], copyright 2022, Springer Nature. (c, d) The HCOOH oxidation path and structure of intermediates on (c) Ir nanocluster, and (d) Ir-N_4-C catalyst. Reprinted with permission from Ref. [70], copyright 2020, Springer Nature.

reported a Fe_2O_3-supported Au single atom as a CO preferential oxidation catalyst, in which the H_2 splitting with a larger energy barrier while CO oxidation with a small energy barrier, the catalyst thus exhibited excellent CO preferential oxidation selectivity. Besides, due to this character, the SAC shows a unique mechanism in the advanced oxidation process. The singlet oxygen is proved to be generated with high selectivity from adsorbed dioxygen or peroxymonosulfate on SAC due to their unique geometry structure, which means SACs are promising in selective oxidation [68]. Shang et al. [69] reported an Al_2O_3-supported Pd single catalyst for high-efficiency cinnamyl alcohol oxidation. During the catalytic process, the singlet-O_2 formed on Pd_1 site and further oxidizes the partially dehydrogenated intermediates, the Pd_1/Al_2O_3 thus shows higher activity and selectivity in cinnamyl alcohol oxidation than the Pd nanoparticle. In addition, SAC was also reported to regulate the reaction path of HCOOH electro-oxidation oxidation. Compared with Ir nanoparticles that suffer from CO* intermediate poisoning (Fig. 5(c)), HCOOH oxidation on Ir-N_4 SAA goes through a none-CO* path and shows excellent HCOOH oxidation activity (Fig. 5(d)) [70]. Similarly, the HCOOH oxidation on Rh-NC SAC also shows excellent activity than Rh nanoparticle [71].

The unique adsorption structure of the reactant on SAA was also reported beneficial for the activation process of the reaction. It is well accepted that the activation of reactant is affected by the adsorption energy of the reactant. For example, the activation of CH_4 molecules needs strong binding between CH_4 and the metal site [64] (Fig. 6(a)). However, too strong binding between CH_4 and catalytic site could result further over oxidation of CH_4 to CO_2 rather CH_3OH. On SAA, such as $AgPt_1$, the CH_4 is adsorbed on Pt single site and then activated to CH_3 with a low energy barrier. The formed CH_3* is adsorbed on the bridge site between Pt and Ag site and shows weak binding strength, thus resulting in the desorption of CH_3* rather than over-oxidation to CO_2 product (Fig. 6(a)). This is because Cu site shows weak adsorption nature while Pt site shows strong adsorption, the adsorption of the reactant is on Pt site while the adsorption of the intermediate is on Ag-Pt bridge site, the strong binding between the reactant to Pt site and weak binding strength between intermediate to Ag-Pt site is thus achieved. Based on such a rule on SAA, the activation of reactant and prevention of over oxidation can be achieved. Besides, the selectivity hydrogenation on SAA also shows different reaction paths than pure metal catalysts. For instance, the oxidation of methanol possibly goes through two different reaction mechanisms, the d-CH_3OH path and the h-CH_3OH path (Fig. 6(b)). On Rh_1Ag (111) SAA, the reaction barrier of CH_3OH activation of the d-CH_3OH path (0.41 eV) is much lower than the h-CH_3OH path (0.71 eV) and on the pure Ag (111) surface (1.2 eV), indicated that construct SAA is a

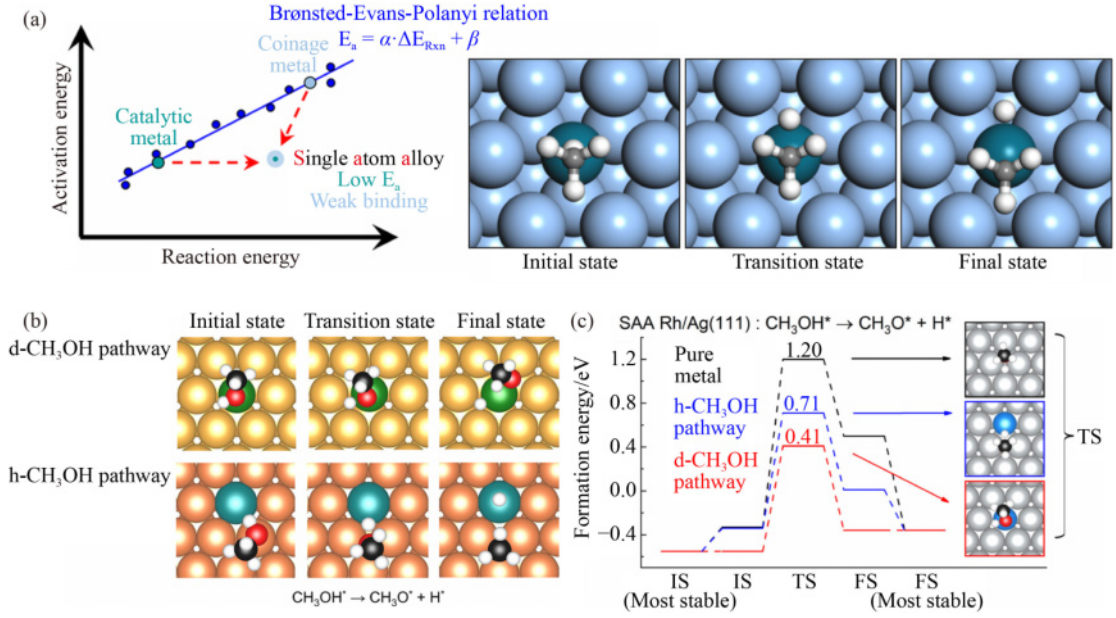

Fig. 6 (a) The scaling relation of reaction energy (*x*-axis) and activation energy (*y*-axis) on the nano metal catalyst and SAA (left), and the structure change of CH_4 dehydrogenation to CH_3* + H* on SAA (right). Reprinted with permission from Ref. [64], copyright 2018, American Chemical Society. (b) The structure schematic of intermediates and (c) free energy change of CH_3OH dehydrogenation on metal and SAA surface. Reprinted with permission from Ref. [72], copyright 2023, American Chemical Society.

useful method to regulate reaction path and facilitate reaction activity [72] (Fig. 6(c)).

In summary, the adsorption structure of reactant and intermediates determined the reaction path, which is highly affected by the local isolate site on SACs. Rational designing of the local structure of the single atom facilitates the activation of the reactant, regulation of the reaction path, and operation of the new reaction process, as well as the synthesis of new reaction products, can be achieved possibly.

2.3 Synergy effect on SACs

SACs with isolate active sites gain the advantage of activation of reactant and selective adsorption of intermediates while being insufficient in catalyzing complex reactions. In complex chemical reactions involving bond cleavage and coupling, multi-site synergy is crucial for SACs. Indeed, the synergistic effect in SACs plays a significant role in regulating their performance. This includes optimizing electronic structure, breaking scaling relations, and catalyzing complex reactions, specifically synergy in bond cleavage and coupling [73,74]. In this section, to focus on the precise regulation of the reaction path, we will deeply discuss the synergy effect of SAC in catalyzing complex reactions from the aspect of bond cleavage and coupling.

Theoretically, it is challenging for an isolated single site to catalyze complex reactions involving bond cleavage or coupling. For instance, Dong et al. [75] reported that a Pd cluster supported on nanodiamond can catalyze the dehydrogenation of dodecahydro-*N*-ethylcarbazole, while a Pd single atom shows no catalytic activity. Another typical example is the electrochemical reduction of CO_2 to C2 products, which is a challenge for SACs due to the unattainable C–C bond coupling process. However, many reports demonstrate that SACs can catalyze complex reactions with excellent performance, such as CO oxidation reaction [76,77], NO_3^- reduction reaction [55,78,79], and CH_4 selective oxidation reaction [80]. This is attributed to the synergy effect between the single site and the coordination atom during catalysis [44].

To introduce a synergy effect in SAC, constructing another metal site near the catalyze site is a useful method. Similar to the electrochemical reduction of CO_2, the formation of C2 products by photocatalytic CO_2 requires multi-sites to facilitate C–C coupling. Jia et al. [81] reported a NiCo-TiO_2 dual-atom catalyst, which shows a lower C–C coupling energy barrier and CO_2 activation energy barrier than Ni-TiO_2 and Co-TiO_2 (Figs. 7(a) and 7(b)). It is noteworthy that C–C coupling can occur on Ni-TiO_2 and Co-TiO_2 SACs but with a higher energy barrier, indicating that the metal oxide support can act as an active site and participate in the coupling process. Due to the synergy between Ni and Co atoms, NiCo-TiO_2 exhibits a lower free energy barrier of C–C coupling than Ni-TiO_2 and Co-TiO_2 (Fig. 7(c)). Therefore, regulating metal-metal synergy is a reasonable method to optimize the performance of a single site. Chu et al. [82] synthesized SiC-supported Pd-based catalysts with different loading. Only isolated Pd single atoms were observed on Pd/SiC-0.5%, while neighboring Pd

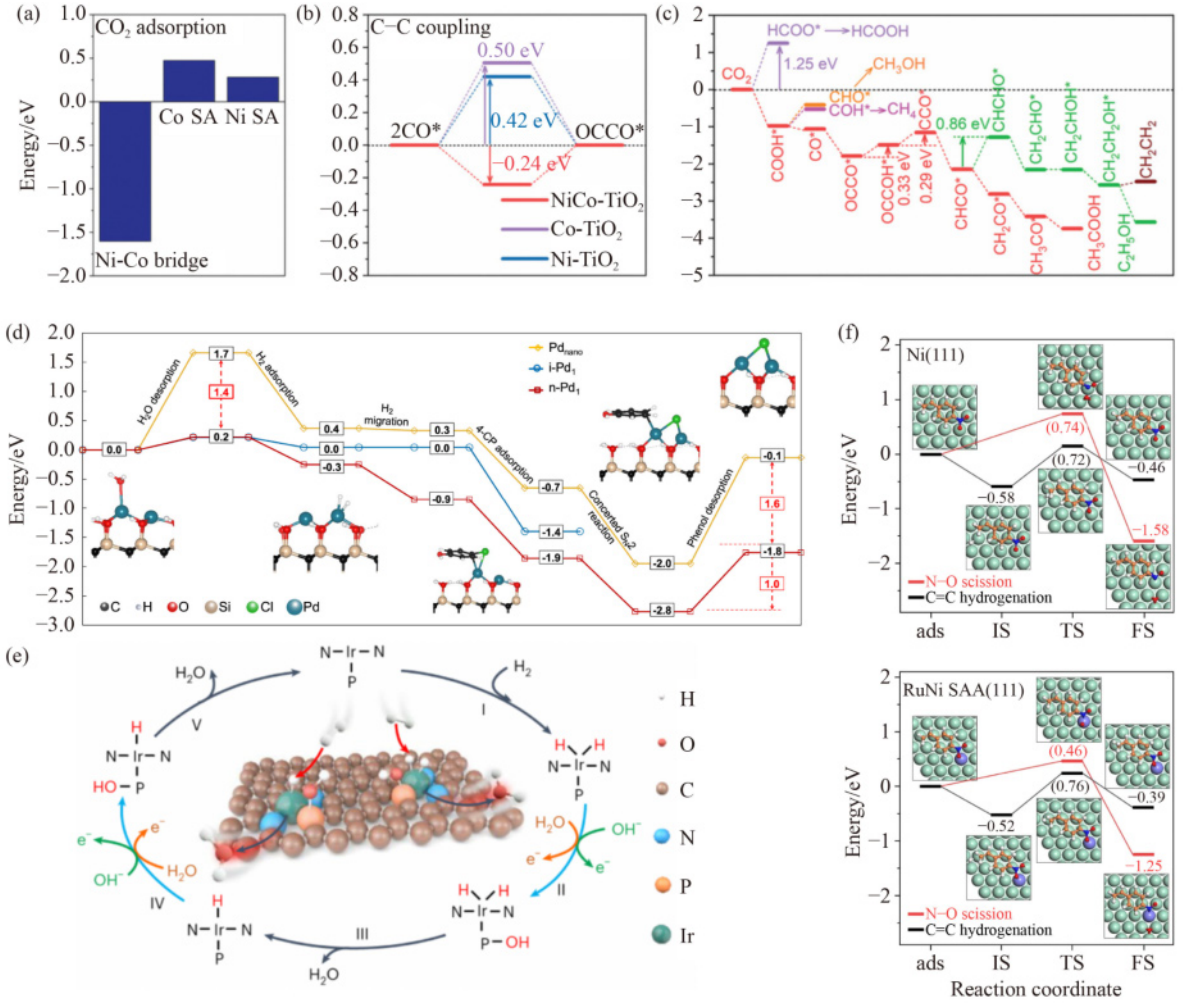

Fig. 7 (a) The adsorption energy of CO_2 on Ni-Co dual atom, Co single atom, and Ni SACs. (b) C–C bond coupling energy on Ni-Co dual atom, Co single atom, and Ni SACs. (c) The CO reduction free energy profile on Ni-Co dual atom catalyst. Reprinted with permission from Ref. [81], copyright 2024, John Wiley and Sons. (d) Hydrohalogenation energy barrier on different Pd sites. Reprinted with permission from Ref. [82], copyright 2021, Springer Nature. (e) The atom structure changes during HOR process on Ir-P atom pair. Reprinted with permission from Ref. [58], copyright 2023, Springer Nature. (f) Chemoselective hydrogenation of nitroarenes on Ni (111) and RuNi (111). Reprinted with permission from Ref. [85], copyright 2022, Springer Nature.

atoms were observed on Pd/SiC-1% and Pd/SiC-5.6%. The experimental results show that neighboring Pd single atoms can cleave the carbon–halogen bond, a process difficult for Pd single atoms or metallic Pd nanoparticles. Density functional theory (DFT) calculation results verified that the neighboring Pd sites show a lower hydrohalogenation energy barrier compared to Pd single-atom sites and Pd (111) surface. Besides, the rational design of synergy between the metal site and a nonmetal is also useful for regulating the reaction path (Fig. 7(d)). Recently, Wang et al. [58] reported an Ir-P atom pair in which the Ir and P atom synergy works to achieve excellent H_2 oxidation reaction performance (Fig. 7(e)). H_2 oxidation reaction, a half-reaction of a fuel cell, is a reversible reaction of H_2 evolution reaction. In general, a nano catalyst of hydrogen evolution reaction (such as Pt) can also catalyze H_2 oxidation reaction. However, single atoms can exhibit excellent H_2 evolution reaction performance, while few SACs can catalyze the H_2 oxidation reaction process. Based on benchmark experiments, the P site is proven to be significant during H_2 oxidation reaction. DFT calculation results indicated that the H_2O is easily cleaved on the P site, forming a P–OH structure. The P–OH combines with Ir–H to form H_2O, enabling the H_2 oxidation reaction process to occur on the Ir-P atom pair.

In addition, the synergy between the metal site and the support can also promote bond coupling or cleavage. Liu et al. [83] reported an MgO (111) supported Ir single atom, which can couple benzene and ethylene to form styrene. Conversely, when the Ir atom is supported on MgO nanoparticles, ethylbenzene is the main product. Except for simple C–C or H–O coupling, when the reaction step is complex, the site needs to cleave some intermediates while coupling others, posing a challenge for a single site. For instance, in hydroformylation reaction, both C–C bond coupling and H–H bond cleavage

occur during the reaction process. The rational design of a dual-atom site to achieve both coupling and cleavage ability can theoretically enhance hydroformylation efficiency. Ro et al. [84] reported an Al_2O_3-supported Rh-W dual atom catalyst for hydroformylation. It is first proved that the Rh-W dual site consists of $Rh(CO)_2$ and W (+5) under the reaction conditions. C_2H_4 is adsorbed on the W (+5) site and then transferred to the Rh site. Subsequently, H_2 is adsorbed on the Rh site and split into two H* atoms on the Rh-W interface, with one H atom adsorbing on Rh and the other on the Rh-W interface. CO can be adsorbed on the Rh site due to the hydrometallation state of Rh. In this state, the CO and a C_2H_4 molecule are adsorbed on the Rh site, facilitating C–C coupling within the Rh site, and leading to the formation of a CH_2CH_2CO* intermediate. This intermediate subsequently transforms into the product CH_3CH_2COH. This study comprehensively demonstrates the significance of synergy sites in complex reactions.

Synergy effects are also evident in SAA catalysts. Liu et al. [85] reported a RuNi SAA for the chemoselective hydrogenation of nitroarenes. The single Ru site on the Ni surface not only activates and cleaves the N–O bond with a low energy barrier but also promotes the formation of key intermediates. This synergy results in the high activity and selectivity of the chemoselective hydrogenation of nitroarenes (Fig. 7(f)).

Synergy effects are widespread in different types of SACs and play significant effects on regulation and facilitate catalyze performance, which include (1) synergy between metal and nonmetal atoms in supported SACs; (2) synergy between metal and support in metal oxide-supported SACs; (3) synergy between two metal-metal sites in dual atom catalysts; (4) synergy in SAAs. Through the rational design of synergy sites, complex reaction processes on SACs can be achieved.

Overall, the precisely controlling reaction pathways via the rational designed of SACs deserves a multifaceted effort. It hinges primarily on the regulation of electronic structure of metal site, which not only facilitates the activation of reactant molecules but also governs the adsorption structure of intermediates, thereby regulate the course of the reaction pathway. The influence of isolated metal sites on the reaction pathway is notable on certain occasions owing to their distinctive adsorption characteristics, rendering them pivotal considerations in SAC design. Furthermore, the construction of atom pairs assumes significance in catalyzing complex reactions, as it fosters both bond coupling and cleavage, while concurrently assisting in reactant activation.

3 The progress of precise catalyzing reactions on SACs

SACs were applied in different kinds of reactions and showed high activity and selectivity. In this section, to correspond with the intrinsic reasons that SAC is skilled in precise catalyze reactions (discussed in section 2), we choose four important reactions to elaborate on the recent progress, including two important electrochemical reactions: ECO_2RR and C–N bond coupling synthesis urea. In such two reactions, both activation of reactant and bond coupling are important. Then, the progress of two important thermocatalysis reactions were introduced: CO_2 hydrogenation reaction, and CH_4 conversion. These reactions include the processes of precise activation of small molecules like CO_2 and CH_4, selectivity oxidation, selectivity reduction, and bond coupling, which cover the main kinds of reaction processes.

3.1 SACs for electrocatalysis reactions

3.1.1 ECO_2RR

To address the energy and environmental challenges stemming from excessive CO_2 emissions, significant attention is being devoted to advancing catalytic technologies for converting CO_2 into valuable chemicals. When driven by electricity, CO_2 can be transformed into C1 products CO, HCOOH, CH_4, CH_3OH, or C2 and C3 products. The three key challenges in these CO_2 conversion processes lie in activating the CO_2 molecule, hydrogenation sites controlling, and facilitating C–C bond coupling. In this section, we will provide a comprehensive summary and discussion of the advancements in precisely controlling the reaction process during ECO_2RR using SACs.

The main C1 products of ECO_2RR are CO and HCOOH, the difference between these two-products generation process are the activation type of CO_2 and binding energy toward reaction intermediates (COOH*/HCOO*), once the activation type of CO_2 and formation of intermediates is controlled, the products selectivity of CO/HCOOH are controlled. Compared with nanocatalysts, many kinds of SACs show high CO or HCOOH product selectivity, for example: (1) N coordinated metal site (M-NC) are excellent catalysts to generate CO product with no HCOOH and few H_2 [86]; (2) CuM_1-SAAs (Sn, Sb, In) can convert CO_2 to CO with a high selectivity, which is quite different to pure Cu or Cu oxide have multi products [87,88]; (3) MCu_1-SAA (Sn, Bi) can achieve high-efficiency ECO_2RR to HCOOH process [88]. In general, the ECO_2RR process on these SACs shows high product selectivity and lower partial HER current density, which could be attributed to the unique electron and geometry structure of the single site.

Here, we want to choose three typical examples of SAC to elaborate on the precise activation of CO_2 toward C1 products. The first one is CO_2 reduction to CO on Ni SAC, in which the CO_2 activation method is different from other M-NC catalysts. Yang et al. [89] synthesized Ni SAC by pyrolyzing Ni with amino acid and melamine.

The synthesized Ni single atom has 9 electrons in the *d*-band and shows a Ni(I) state, different from the typical Ni(II) in NiPc molecule with 8 d electrons. During CO_2 reduction, once the CO_2 adsorbed on Ni(I) site, The *d*-band electron of Ni site offers an electron to CO_2, and the CO_2*$^{-}$ thus easy to transform to COOH* and achieve a fast ECO_2RR process ultimately, the A-Ni-NSG thus shows higher CO selectivity and lower overpotential (Figs. 8(a) and 8(b)). Such work proved the valence state of a single atom site is confined by its coordination environment and eventually affects the catalyze performance.

In general, the ECO_2RR on M-NC SAC converts CO_2 to CO without HCOOH products, such as CO_2RR on FeNC, CoNC, NiNC, and MnNC. However, in some reports, Sn-NC catalysts show different products, both CO and HCOOH products are reported. To expound the essential reason, we investigated the CO_2 reduction process in a model O-Sn(IV)Pc-CNT-OH catalyst, in which the O-Sn atom pair shows an important role in catalyzing selectivity regulation [90]. When the CO_2 adsorbed on O-Sn atom pair, the CO_3* structure formed. Then the CO_3* structure transforms to HCOO* and eventually forms HCOOH product. Compared with Sn(II)Pc produces CO product, the existence of Sn-O atom pair is important in the process of CO_2 to HCOOH (Figs. 8(c) and 8(d)).

Besides, even though the CO_2 to C2 product process is considered as happening on Cu nano catalyst in general. A single atom site with a suitable coordination environment can also generate C2 product during ECO_2RR with local multi-site synergy, such as ECO_2RR on a Sn-O_4 site [91]. The Sn-O_4 site is synthesized in a hydrothermal method and has three coordinate O atoms on a carbon support and an OH group axially. When the catalyst is applied potential, the OH-Sn-O_3 changes to Sn-O_3 at first, then the CO_2 is adsorbed on Sn site and forms a Sn-O_3-COOH and further reduces to Sn-O_3-CHOH. Then a CHO* space is generated from a tandem SnS_2 catalyst adsorbed on Sn site and further reduced to CH_2*. At this time, a Sn site can adsorb two different C species and C–C bond coupling happening then generate C2 product ethanol.

As for the C–C bond coupling process during ECO_2RR to C2 products, Cu-based nanomaterials are the most common catalysts. Even though pure Cu can generate C2 products during CO_2RR, however, the product distribu-

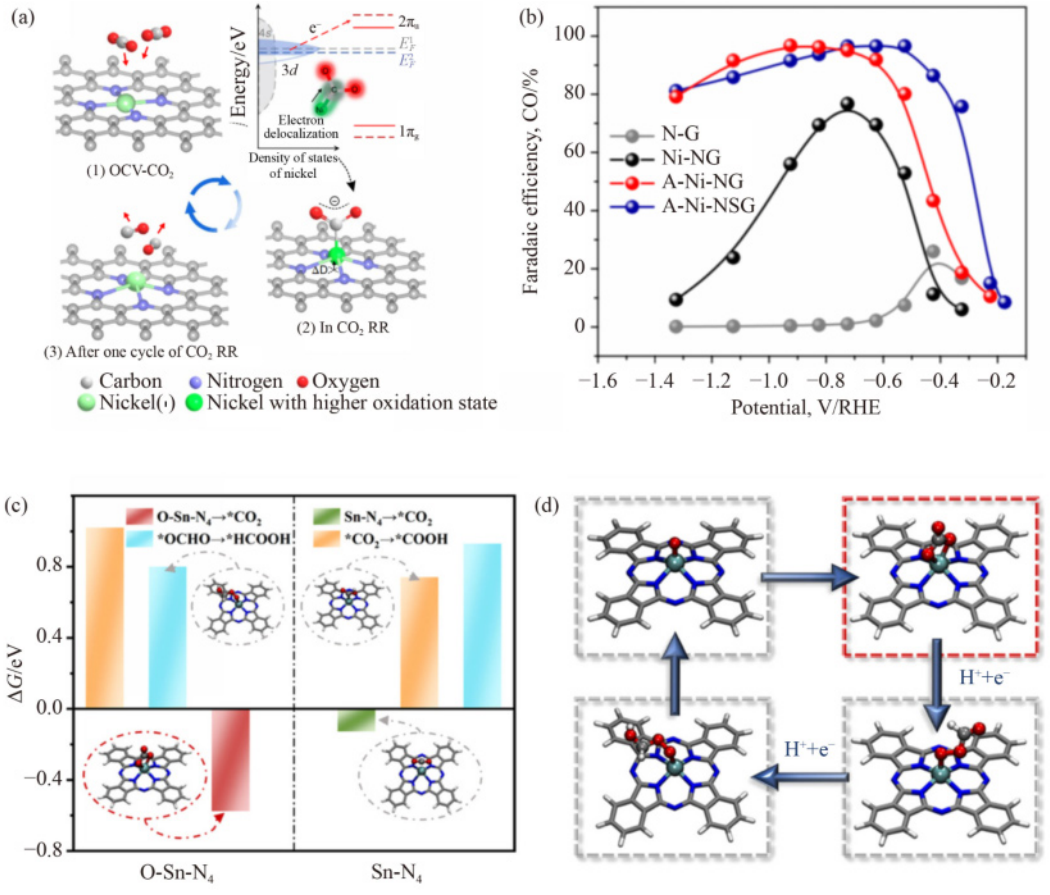

Fig. 8 (a) The electronic structure of Ni(I)N_4 site and the corresponding CO_2 activation mechanism. (b) The CO_2RR product selectivity of four different Ni-based SACs. Reprinted with permission from Ref. [89], copyright 2018, Springer Nature. (c) The adsorption structure and energy of CO_2 on Sn(II)Pc and O-Sn(IV)Pc catalysts. (d) The CO_2RR process on O-Sn(IV)Pc catalyst. Reprinted with permission from Ref. [90], copyright 2023, American Chemical Society.

tions are spread. Constructing SAA is a useful method to regulation the product distribution of Cu catalysts. For example, when adding Sb, Sn, and In atoms to the Cu matrix, the selectivity of CO product increases prominently, even though Sb [87] and Sn-based catalysts [92] are not good ECO_2RR to CO catalysts. The reason behind this is the unique electronic structure on a single-atom metal site is good at the activation and conversion of CO_2.

However, when adding Bi to Cu matrix, the results are quite different. Two similar results were reported on Bi-doped Cu-based SAA that Bi doping is beneficial for C–C bond coupling and enhancing C2 product selectivity [93,94]. For example [94], Bi decorated CuS nano flower were first synthesized in a hydrothermal method and then *in situ* reduction to BiCu-SAA at –0.9 V. The total Faraday efficiency (FE) of C2 product at –1.1 V was 73.4%, much higher than the benchmark Cu catalyst (41.9%). *In situ*-SEIRAS results proved CO* on BiCu-SAA is easy to transform to C2 products which is in contrast to Cu nano catalyst. DFT calculation results proved the Bi atom not only facilitates the formation of CO* by enhancing the binding energy of COOH* but also promotes C–C bond coupling from COH* and CO* to COHCO*.

In conclusion, the performance of ECO_2RR on different Cu-based SAA are quite different, even though only 0.5%–1% metal atom is exposed over Cu surface, the product distribution change from multi-product to single C1 product or high selectivity C2 products. The mechanism of single atom site modifies ECO_2RR performance of Cu matrix still needs to be investigated to gain a universal guide rule.

3.1.2 Urea electro-synthesis

Urea is an important chemical in industry synthesis which is synthesized by a reaction of CO_2 and NH_3 at high temperature and pressure. In the electrochemical method, urea can be generated with a C–N coupling process by using CO_2 as the C source and N_2 or NO_3^- as the N source.

3.1.3 C–N coupling to urea using NO_3^- as N source

When using NO_3^- as the N source, the NO_3^- is first reduced to NO/N/NH/NH_2* intermediate and then coupled with CO and form a urea product [95]. It is easy to accept that the catalyst should have the ability to form CO intermediate from CO_2 to CO, generate N* intermediates from the reduction of NO_3^-, and bond coupling of C–N [96]. Recently, Zhang et al. [96] reported an N atom coordinated Fe-Ni dual atom catalyst for efficiency C–N coupling and generating urea product with high selectivity. The Fe-SAC, Ni-SAC, Fe–Ni mixed diatomic SCA, and Fe–Ni pairs DAC were both synthesized. The Fe–Ni pairs show higher urea yield rate and selectivity than the other three isolated Fe/Ni catalysts due to the synergy between Ni and Fe site, in which the Fe site can generate NH* intermediate while Ni site can generate CO*. Besides, the close distance of the Fe–Ni site is beneficial for the coupling of C–N bond. DFT calculation results show that the Fe-Ni pairs can adsorb and activate NO_3^- and CO_2 with lower energy barriers than Fe-SAC, Ni-SAC, and i-FeNi-SAC. Besides, the adjacent FeNi sites accelerate the C–N coupling and result in a lower C–N coupling energy barrier eventually. Such an investigation proved the importance of CO formation, NO_3^- reduction, and C–N coupling during urea electrosynthesis (Figs. 9(a) and 9(b)).

Similar to C–C bond coupling during CO_2 can happen on Cu-based catalysts, Cu-based catalysts also have the ability of C–N coupling to synthesis urea in aqueous solution. However, the poor ability of CO* formation limits the product selectivity of urea (less than 5%). Hence, increasing the ability of CO_2 to CO is a potential method to increase the urea product selectivity. Wang et al. investigated the co-reduction performance of CuM_1 SAA in which the M doping can accumulate the formation of CO*. As discussed above (ECO_2RR section), the doping of Sn, Bi, and In atoms on Cu nanoparticles can facilitate the formation of CO*, it is thus possible also beneficial for the generation of urea product in CO_2 and NO_3^- co-reduction. They investigated the CO* intermediate formation ability of CuM SAA to affect the efficiency of urea product yield rate [97]. Compare with CuM alloys (CuBi, CuIn, CuSn) with lower Cu amounts that tend to generate HCOOH product in CO_2 environment, CuM_1 SAAs tend to generate CO* product. When adding NO_3^- in solution, the formation of urea on CuM_1 SAA is obviously easier than on CuM alloy. Such a result proved the importance of CO* intermediate on Cu surface during C–N coupling process (Fig. 9(c)).

In short, the C–N bond coupling on the surface of the catalyst is limited by three abilities of the catalyst. (1) The ability of formation of CO* intermediate. Such a process is important for the synthesis of urea. Because the formation of CO is a 2e process, while the formation of urea is a 16e process. When the coupling of CO* increases by 1%, the FE of urea increases by 8%. (2) The ability to reduce of NO_3^-. As for the C–N bond coupling, the C source is from the CO* intermediate, while the N source is still not clear, it may be NO*, NH*, NH_2*. Further investigation should also be paid on the aspect of NO_3^- reduction, clearing the C–N coupling intermediate and finding the ruler of C–N coupling on different N intermediates is helpful for further catalyst design. (3) The ability of C–N coupling. The current investigations main focus on the formation of CO* intermediate, while the investigation of C–N coupling process is missed. It still needs further investigation in this field to explain and guide the catalyst design.

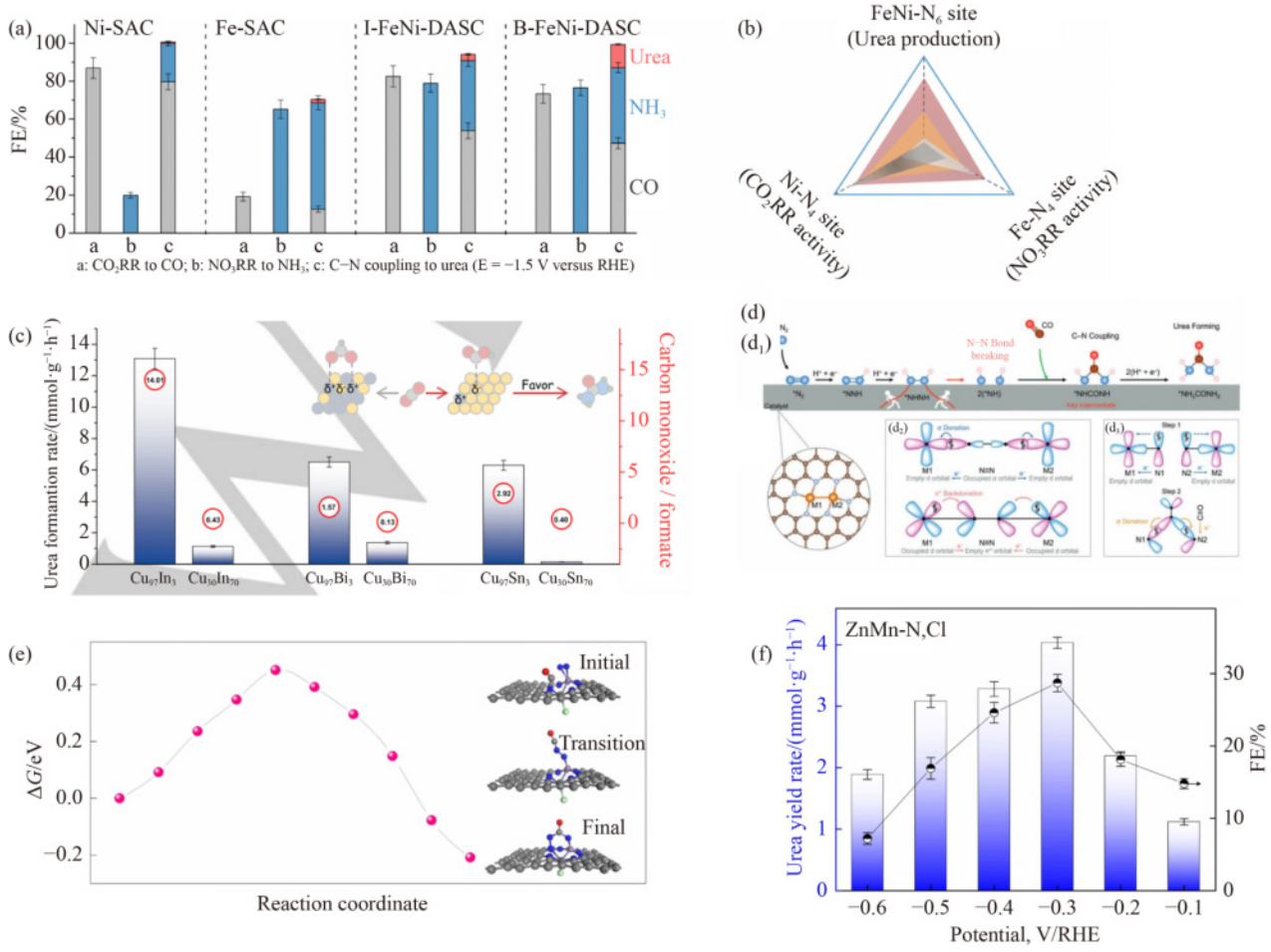

Fig. 9 (a) The FE of urea on Fe single atom, Ni single atom, Fe/Ni dual single atom, as well as FeNi dual catalysts. (b) The summarize of CO_2RR and NO_3RR and co-reduction performance of Ni single, Fe single, and FeNi dual atom catalysts. Reprinted with permission from Ref. [96], copyright 2022, Springer Nature. (c) The performance of urea yield of CuM alloy with different M amounts (M = Bi, Sn, Sb). Reprinted with permission from Ref. [97], copyright 2023, John Wiley and Sons. (d) The schematic of N_2 and CO_2 co-reduction on M_2N_6 dual atom catalysts. Reprinted with permission from Ref. [99], copyright 2023, John Wiley and Sons. (e) The free energy profile and structure of N_2-CO coupling on ZnMn dual atom catalyst. (f) The FE of urea on the different potential of ZnMn dual atom catalyst. Reprinted with permission from Ref. [100], copyright 2023, John Wiley and Sons.

3.1.4 C–N coupling to urea using N_2 as N source

Different from NO_3^- as the N source, when using N_2 as the N source, there are two different reaction mechanisms. On one hand, the N_2 can be reduced to NH intermediates and then coupling with CO and generate urea [98]. However, such a process is limited by the stable N–N bond cleavage process. On the other hand, the N_2 can hydrogenation to HNNH* intermediate and then coupling with CO to form HN-CO-NH* intermediate and then reduce to urea without N–N bond cleavage process. Hopefully, the urea synthesis can happen based on this reaction mechanism with high N_2 efficiency (near 100%), low energy barrier, and high urea selectivity.

From the aspect of theory calculation guide catalyst design, such a process is reasonable and investigated by Liu et al. [99] They proposed a synergistic process of urea synthesis based on co-reduction of N_2 and CO_2. Different form N_2 reduction to NH_3 the N–N bond cleavage is a challenge, N–N bond cleavage with the help of CO insert is much easier and thus shows low C–N bond coupling and N–N bond cleavage energy barrier for highly efficient urea production (Fig. 9(d)). The calculation results predict that V_2-N_6C is a suitable catalyst to adsorb N_2 on V site. The adsorbed N_2 is activated and hydrogenated to HNNH* then coupling with CO eventually forming a urea product with a low energy barrier. This study presents a new avenue for developing novel mechanisms and efficient catalysts for urea electrochemical synthesis. Zhang et al. [100] proved such a process from the aspect of the experiment. They synthesized a ZnMn dual atom catalyst with six N coordination in plane and axial chloride coordination. The ZnMn-DAC shows excellent urea product yield and super high N-selectivity during urea synthesis. In other words, no obvious NH_3 is formed during the urea synthesis process. The reaction begins from the adsorb of N_2 on the metal site and forms a plane adsorb structure, the CO* then couples with N_2 and forms

a N–CO–N structure, the stable N–N bond cleavage in this step, which is different from the N_2 reduction process that the N–N bond is difficult to be cleavage. Therefore, the co-reduction of N_2 and CO_2 to form urea happens in a low overpotential rather than a high overpotential like N_2 reduction (Figs. 9(e) and 9(f)).

In short, the N_2 and CO_2 co-reduction on the catalyst is proved from the aspect of theory calculation and experiment, even though the specific reaction path still needs more investigation from the aspect of experiment and theory calculation, the reaction mechanism of urea synthesis with no N–N bond cleavage is possible. Further, the detailed and universal reaction mechanism should be investigated to guide the catalyst design of urea synthesis.

3.2 SACs for thermocatalysis reactions

3.2.1 CO_2 hydrogenation

Except for the drive by electric energy, CO_2 can also convert to high-value-added chemicals in the drive of heat and use H_2 as the H source. Similarly, CO_2 hydrogenation is also a challenge in the aspect of CO_2 activation, and C–C bond coupling. Differently, the H source of hydrogenation is from H_2, the activation of H_2 is thus also important during CO_2 hydrogenation.

CO is one of the most attractive products in CO_2 hydrogenation, such a process is named as reverse water gas shift reaction. The challenges of such a process are the CO_2 adsorption and activation process, as well as the prevention of over-hydrogenation of CO product to CH_4 or CH_3OH. SACs, such as metal oxide-supported single-atom sites show excellent performance of reverse water gas shift in many reports [101−103]. Yang et al. [104] investigated the size effect of Re site supported on TiO_2 from single level to cluster toward CO_2 hydrogen to CO. The Re SAC and Re cluster were synthesized by controlling the amount of Re element when support on TiO_2 support. It is clear that the product distribution (CO/CH_4) changed from CO to CH_4 with the increasing of Re size. Compared with Re cluster that can convert CO_2 to CH_4, CO_2 tends to be reduced to CO on Re SAC. Besides, the CO_2 conversion rate also increased with the increasing of Re size because more Re sites existed in Re cluster. Based on *in situ* Fourier transform infrared and DFT results, the CO_2 hydrogen process of on Re single atom is stopped when CO is generated, while the CO can be further hydrogen to CH_4 on Re cluster edge site. Except for metal-oxide supported isolate metal site, C_3N_4 supported metal site can also catalyze hydrogenation of CO_2 to CO. Wang et al. [105] investigated the reverse water gas shift performance on Ni-C_3N_4 SAC, which shows almost 100% CO product selectivity and a STY of 1.88 $mol_{CO}\cdot g_{Ni}^{-1}\cdot h^{-1}$. The mechanism investigation proved the super high selectivity originates from the strong adsorption energy of CO_2 and weak adsorption of H_2 on Ni site. Similar to ECO_2RR, CO_2 can also hydrogenation to HCOOH on SAC. On Ir single atom site with suitable reaction conditions, CO_2 can be hydrogenated to HCOOH with high selectivity [106]. DFT calculation results indicated the CO_2 first adsorbed and rotated to an O–C–O with a bend of 135°. Then the CO_2* hydrogenation to HCO_2* and further hydrogenation to HCOOH product. Not only Ir SAC, but the CO_2 can also hydrogenation to HCOOH over Ir based complex with a similar coordination environment (Fig. 10(a)).

In addition, the CO_2 can be hydrogen to CH_3OH on a single atom site, to gain a high selectivity CH_3OH product, regulation of the reaction route is important. Huang and coworkers reported two different Cu single atom support on C_3N_4 support, in which the coordination N atom number are 3 and 4 respectively [107]. During the CO_2 hydrogenation process, it tend to go through a formate path and generate CH_3OH product on Cu-N_4 catalyst, while the Cu-N_3 catalyst tend to catalyze CO_2 to CO via a water-gas-shift pathway (Fig. 10(b)). Chen et al. [108] reported Pt single atom coordinated with O atom (Pt_1@MIL) shows a different reaction path and high CH_3OH selectivity compared with Pt_n@MIL. The Pt_1@MIL shows higher ability to deep hydrogen of CO_2 than Pt_n@MIL, which is because the reaction path on Pt_1 and Pt_n are quite different. On Pt_1@MIL, the CO_2 hydrogen to HCOO* intermediate rather than COOH* interaction, which makes the main product is CH_3OH on Pt_1 while CO product on Pt_n.

For the generate of C2 products such as ethanol, C–C bond coupling ability of the catalyst is important. Ir_1-In_2O_3 catalyst was designed and synthesized to convert CO_2 to ethanol with high selectivity [109]. The Ir site is exposed over the surface of In_2O_3 and with an O vacancy near Ir. Beneficial from the exist of Ir and Ov sites, the Ir_1-In_2O_3 can catalyze activation of CO_2 to CO with a lower free energy barrier than In_2O_3. The CO* is then hydrogenation to CH_3O* and adsorbed on Ov site, then coupling with CO* on Ir site eventually resulting in high ethanol product selectivity (99.7%) (Fig. 10(c)). Similarly, the Rh-Ov atom pair supported on Ti-dopped CeO_2 with excellent CH_3CH_2OH selectivity (99.1%) and turnover frequency (TOF) (493.1 h^{-1}) for CO_2 hydrogenation was also reported [110] (Fig. 10(d)). The mechanism investigation proved the reaction begins from the activation of CO_2 on Ov-Rh atom pairs and forms an H_2COOH* intermediate, Then the H_2COOH* transforms to H_2CO* and further hydrogenation to H_3C* intermediates. Beneficial from the synergy effect, the C–C bond coupling further happens on $Rh_1/CeTiO_x$ to generate CH_3CH_2OH products.

3.2.2 CH_4 conversion

The conversion of methane to high-value-added oxygenates has attracted extensive research attention [111,112].

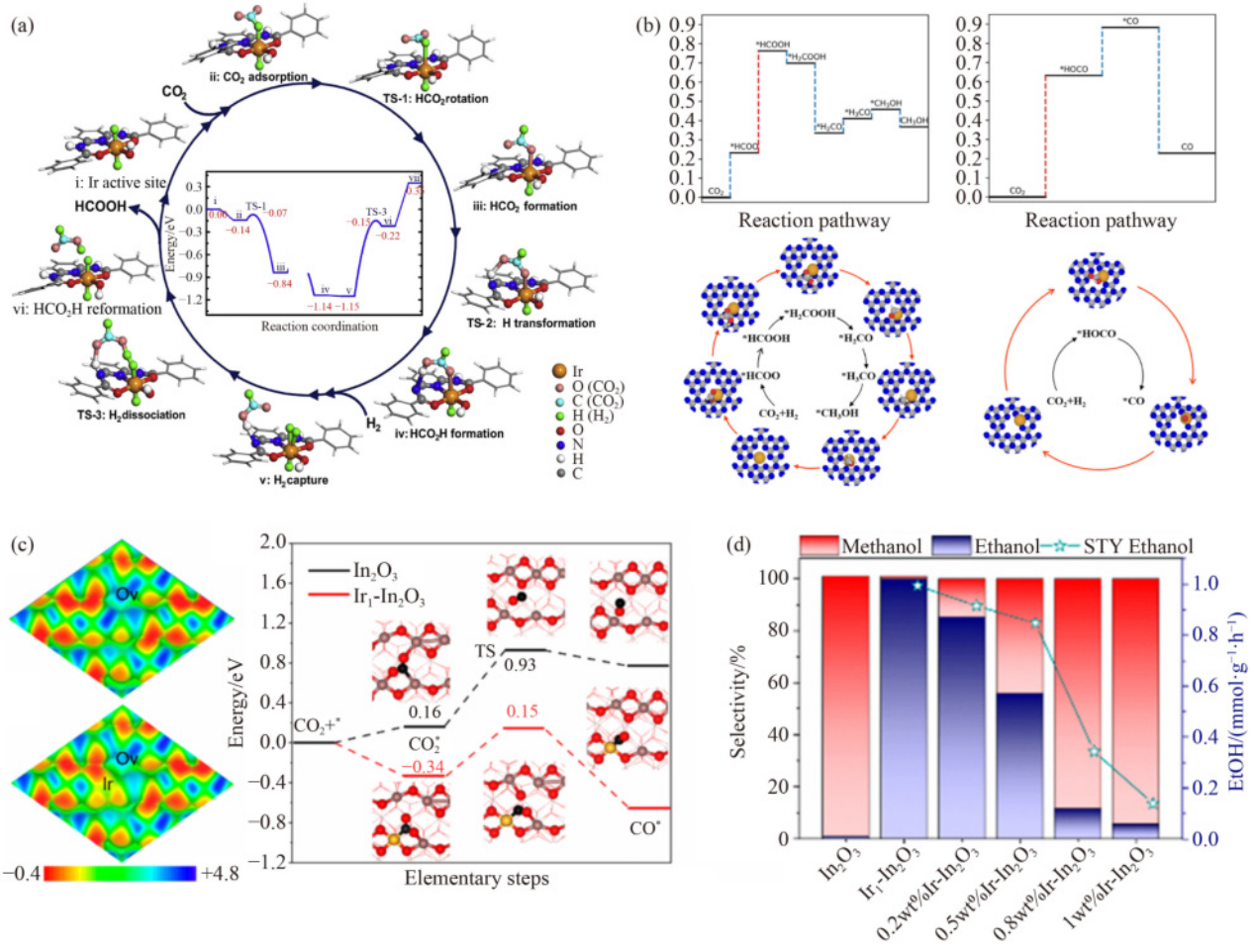

Fig. 10 (a) The reaction process and free energy diagram of CO_2 hydrogenation to HCOOH on Ir single atom site. Reprinted with permission from Ref. [106], copyright 2019, Springer Nature. (b) The reaction path and free energy barrier of CO_2 hydrogen to CH_3OH/CO on Cu-N_4/N_3 catalysts. Reprinted with permission from Ref. [107], 2021, copyright Springer Nature. (c) The electron distribution of Ir-In_2O_3 and In_2O_3 catalysts as well as corresponding free energy diagram of CO_2 hydrogenation to CO. (d) The product selectivity of CO_2 hydrogenation to ethanol on different Ir-In_2O_3 catalysts. Reprinted with permission from Ref. [109], copyright 2019, Springer Nature.

However, such an oxidation process is limited by the challenge C–H bond activation processes, high reaction energy barriers, C–C bond coupling, and susceptibility to overoxidation. Recently, in many reports, SACs can efficiently activate CH_4 molecules and effectively prevent overoxidation [113].

Methanol is a main product of CH_4 oxidation, the key points of the CH_3OH product optimization are the regulation of CH_4 activation and the controlling of CH_4 oxidation degree. The first important point is the activation of CH_4. Supported metal SACs with metal–O coordination are common methane activation catalysts, such as Pd, Pt, Ni, Rh, etc. By regulation the interaction between a single site and support, the activation ability of a single site can be improved. Yang et al. [114] investigated the activation process of CH_4 on $CoFe_2O_4$ support. By a simple water soaking treatment, the H_2O is dissociated and form H^+, which bond with Pt site and weak the interaction between Pt and support. Hence, the charge transfer form support to Pt site is reduced, and the activation of C–H bond is increased. Eventually, the activity of CH_4 activates improved by more than 50 folds. Except for the activation of CH_4, control of the oxidate state of CH_4 is also important. Fang et al. [115] developed a metal-organic framework (MOF)-supported single-atom Ru catalyst (Ru_1/UiO-66), which efficiently converts methane to oxygenates by using hydrogen peroxide as the oxidant. Compared to UiO-66 alone or supported Ru nanocluster catalysts, Ru_1/UiO-66 exhibited nearly 100% selectivity and 185.4 h^{-1} TOF toward oxygenate products, with yields that were an order of magnitude higher than those of UiO-66 alone and several times higher than those of loaded Ru nanoparticles or other conventional Ru_1 catalysts, and showed strong inhibition of over-oxidation. *In situ* characterization and DFT calculations reveal a synergistic effect between the single Ru site and the electron-rich Zr-oxo site of UiO-66 on Ru_1/UiO-66 catalyst. The Ru_1 site is responsible for the activation of

CH_4 via the resulting *Ru_1=O substance, whereas the Zr–O site is responsible for the formation of the oxygen radical substance to produce oxygenated compounds. In particular, the Ru_1-modified Zr-oxo site converts excess H_2O_2 into inactive O_2 rather than Zr–OH radicals, which helps to inhibit the over-oxidation of oxygenated compounds. Similarly, high selectivity CH_4 activation to the CH_3OH process is achieved on Cu-O_4 catalyst [113] (Fig. 11). The investigation proved the effect of CH_4 activation and prevent of over-oxidation of CH_4 on Cu–O_4 site. Besides, the construction of a multi-atom site is a good method to catalyze CH_4 to CH_3OH because such a process concludes processes of CH_4 activation and selectivity oxidation. When Cu atom increases to three, the Cu_3O_3 is proved as the CH_4 conversion site with high selectivity toward CH_3OH [116]. Yu et al. [117] investigated the CH_4 activation process with the help of H_2O_2 on ZSM-5-supported Cu and Ag dual single atoms. The synthesized Ag_1-Cu_1/ZSM-5 hetero-SAC shows a methanol productivity of 20115 μmol·g_{cat}^{-1} with 81% selectivity. The mechanism investigation finds that the synergistic interaction between silver and copper facilitates the formation of highly reactive surface hydroxyl species to activate the C–H bond as well as the activity, selectivity, and stability of Ag_1-Cu_1/ZSM-5 compared with SACs, which is the key to the enhanced catalytic performance. Hence, the rational design dual atom site to facilitate the activation of CH_4 and oxidate to CH_3OH is useful for high efficacy CH_3OH synthesis process.

Similar to ECO_2RR, the formation of C_2 products during CH_4 activation also needs C–C bond coupling process by multi-site synergy. Currently, there are some reports that CH_4 can be activated and converted to C2 products on different kinds of catalysts [118−120]. However, there is still a lack of reports that CH_4 directly converts to C2 product on SACs, which may be attributed to the challenge of CH_4 activation and the C–C bond coupling process. Considering there are many reports of CO_2 reduction to C2 on SACs, further investigation of CH_4 direction selectivity oxidation to C2 product is possibly achieved on SACs.

In summary, the application of SACs in various reactions holds promise. On one hand, SACs exhibit high atom efficiency, resulting in elevated TOF values. On the other hand, the uniform structure of SACs facilitates the enhancement of product selectivity. Importantly, through the regulation of electronic structure and the construction of atom pairs, SACs can effectively catalyze diverse reactions and facilitate complex reaction processes.

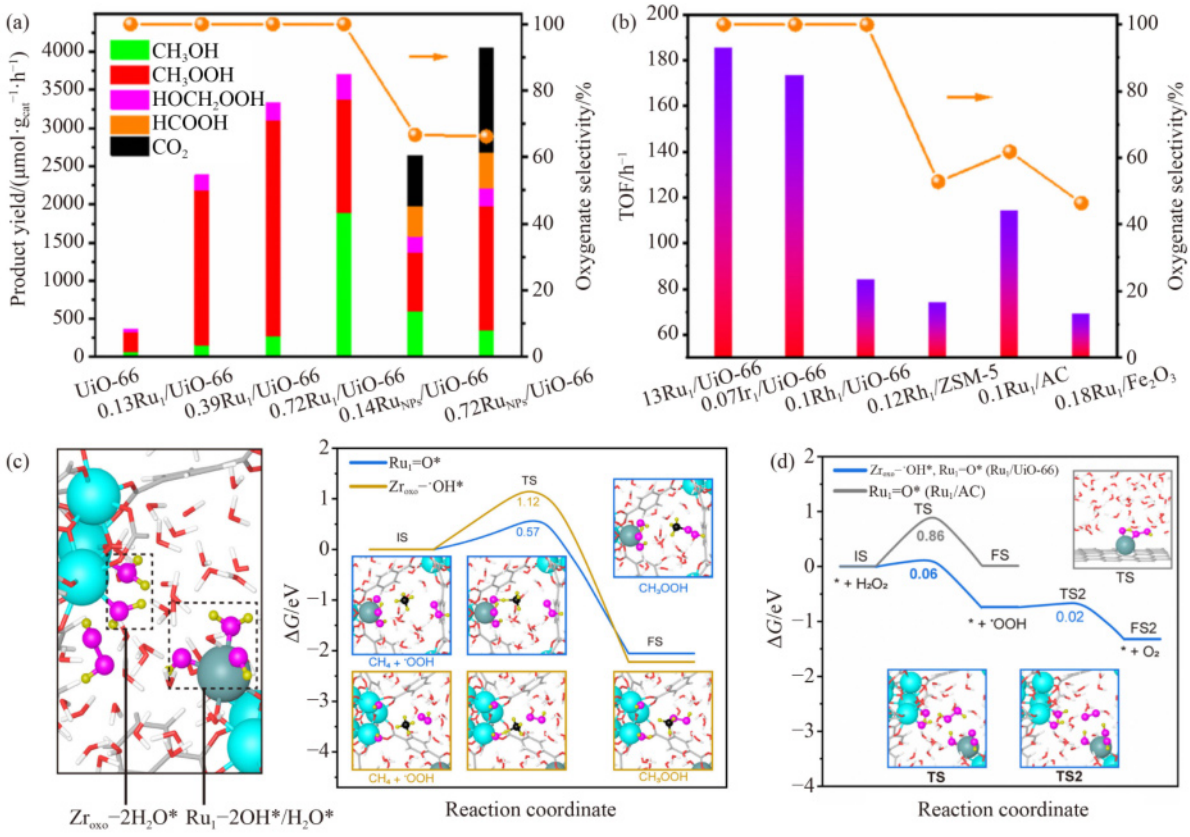

Fig. 11 (a) The product yield and (b) the TOF values of different Ru-UiO-66 catalysts with different Ru state during CH_4 conversion. (c) The model structure of Zr and Ru site during CH_4 activation and corresponding free energy barriers. (d) The free energy barriers of formation of •OOH and O_2 on Zr oxo–•OH* and Ru_1=O* sites. Reprinted with permission from Ref. [115], copyright 2023, American Chemical Society.

4 The importance of support for SACs

In the above sections, we summarized the recent progress of electrocatalysis and thermocatalysis, including ECO_2RR, urea electrosynthesis, CO_2 hydrogenation, and CH_4 activation from the aspect of the local coordination environment. Actually, the performance of SAC is also affected by the structure and performance of support. For example, the CoPc molecular is reported as a catalyst for electrochemical reduction of CO_2 to CO or CH_3OH in some reports. When the CoPc is supported on a single-wall carbon nano tube (SWCNT, d = 1.5 nm), the CoPc-SWCNT can convert electro-reduced CO_2 to CH_3OH, however, when CoPc is supported on CNT (d = 50 nm), the CoPc-CNT tend to catalytic CO_2 reduce to CO (Fig. 12(a)) [121]. The reason behind is the strong interaction between CoPc and SWCNT make the CoPc molecular be curved, the binding energy of CO* intermediate be strong and the convert of CO* to CH_3OH rather than CO* desorption happened. Similarly, the CO_2 hydrogenation to methanol on MoS_2-supported Cu SAC (Cu_1-MoS_2) was also facilitated by curved MoS_2 support [122]. Compared with Cu_1-MoS_2 with no curve, the Cu_1-MoS_2-S (with the curve) shows higher methanol selectivity and activity. DFT calculation results proved the tensile strain appears on the outside surface while compressive strain appears on the inside surface. The electronic structure of the Cu site thus changed and the energy barrier of CO_2 hydrogenation is thus decreased when there is a compressive strain (–2%) and the energy barrier of O hydrogenation increased when there is compressive strain (–2%) (Fig. 12(b)). Hence, the interaction between single atom site and support as well as the structure of the support play significance role in the performance of catalyst (Figs. 12(c) and 12(d)).

In this section, to expound the importance of support in electrocatalytic SACs and thermocatalytic SACs, we discuss the support facilitates SACs performance from the following three aspects:

(1) Channel design of SACs. For catalytic reactions involving a gas-water interface, especially when gas molecular transfer and desorption are involved, it is very important to carry out reasonable structural design of

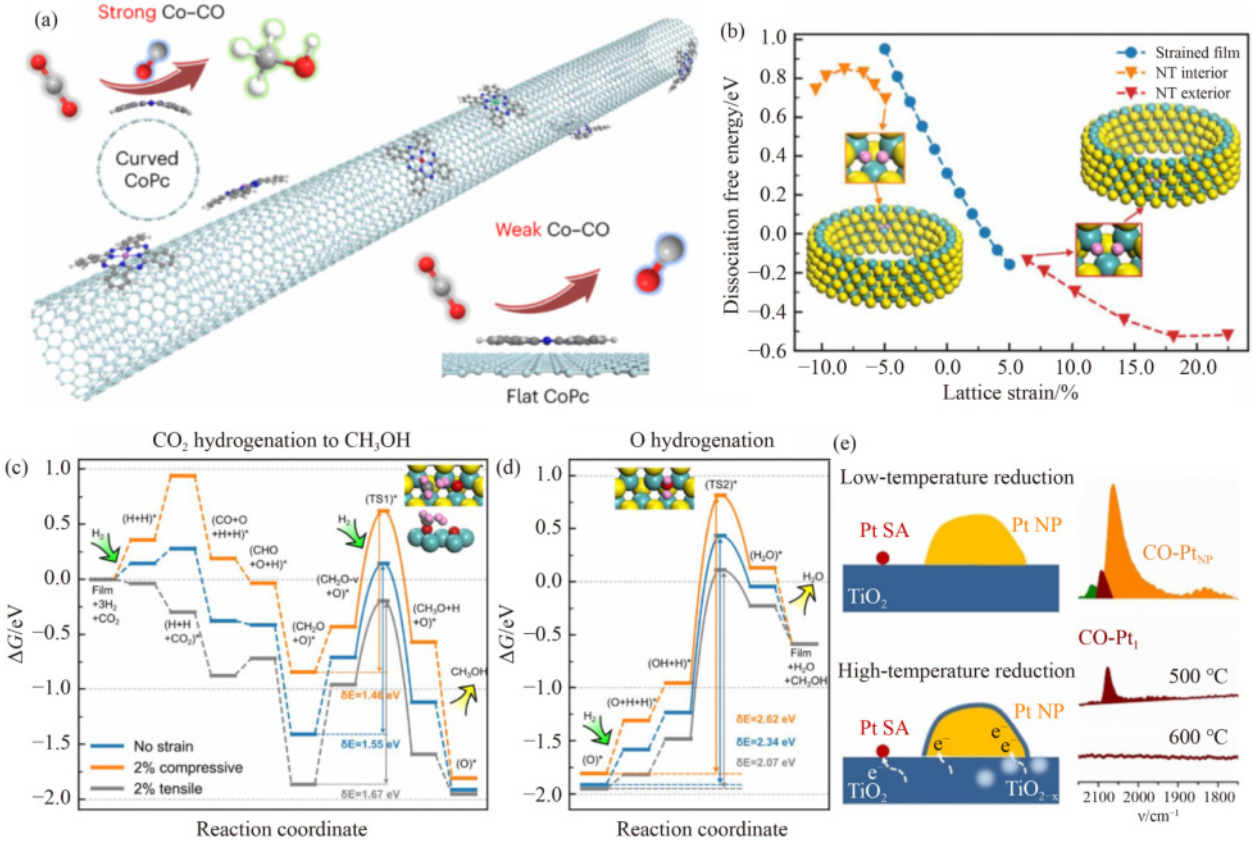

Fig. 12 (a) The schematic diagram of CO_2 reduction to CH_3OH on CoPc catalyst supported on single wall carbon nano tube with tensile strain and plane support with no strain. Reprinted with permission from Ref. [121], copyright 2023, Springer Nature. (b) The relation between energies of dissociative adsorption of H_2 on Sv of strained films and MoS_2 nanotubes. (c) The free energy diagram of CO_2 hydrogenation to CH_3OH on Cu_1-MoS_2 with tensile and compressive strain. (d) The free energy diagram of O hydrogenation on Cu_1-MoS_2 with tensile and compressive strain. Reprinted with permission from Ref. [122], copyright 2023, Springer Nature. (e) The schematic diagram of metal support interaction of Pt single atom and Pt nanoparticle toward TiO_2 support at different temperatures. Reprinted with permission from Ref. [125], copyright 2020, John Wiley and Sons.

catalyst support to promote the transfer of gas molecules. For example, M-NC catalysts with pore structures synthesized by pyrolysis using silica spheres as templates show excellent oxygen reduction reaction and ECO_2RR activity. Such catalyst design ideas are also consistent in thermal catalysis and photocatalysis, such as zeolite-based SACs [123].

On the other hand, the channel structure can also lead to the confinement effect. Deng et al. [124] demonstrated a zeolite-confined Pt SAC for selective hydrogenation of α,β-unsaturated aldehydes to unsaturated alcohols and of nitroarenes to arylamines. The H_2 can easily cleavage to H^+ and $H^{\delta-}$ on Pt site and act as an activated reagent for selectivity hydrogenation.

Therefore, the mass transfer of gas molecules can be improved and the reaction path can be optimized by means of the limited range effect through reasonable channel design.

(2) Support-metal strong interaction (SMSI). SMSI is the key to improving the performance of catalytic sites. On the one hand, the stability of the catalytic site can be improved through the SMSI. On the other hand, the electronic structure of the catalytic site is also affected by the interaction between the metal site and support. In terms of SAC design and precise control of the catalytic process, the SMSI has been shown to optimize the reaction path and product selectivity by regulating the electronic structure of the metal site [126]. Han et al. [125] instigated the SMSI effect on Pt-TiO_2 catalyst. A Pt single atom and Pt cluster co-existed catalyst were supported on TiO_2 support. Compared with SMSI of Pt-NPs-TiO_2, the SMSI on Pt-SAC-TiO_2 occurs at a higher temperature. Hence, the chemoselective hydrogenation of 3-nitrostyrene on Pt/TiO_2 catalyst shows different reaction selectivity and conversion at different temperatures. It is found that over 600 °C, the selectivity is close to 100% and the conversion rate increases gradually (Fig. 12(e)).

(3) The hydrophilic and hydrophobic of support. As for the electrocatalyst design, such as ECO_2RR and electrosynthesis of urea, it is difficult to avoid H_2 evolution reaction competitive reaction. Therefore, in the design of the ECO_2RR catalyst, an important research direction is H_2 evolution reaction inhibition. Hydrophobic treatment of the catalyst surface has been proved to be an effective method for inhibiting H_2 evolution reaction side reactions [127]. O_2 evolution reaction competition also occurs for other electrooxidation reactions in a high potential range (over 1.23 V vs reversible hydrogen electrode), such as 5-hydroxymethylfurfural oxidation and methane electrooxidation. In addition, for some electrocatalytic hydrogenation reactions, such as O_2 reduction reaction, when the reaction potential is higher than H_2 evolution reaction, the reaction is not troubled by H_2 evolution reaction, and the hydrophilic surface support is conducive to the hydrogenation process. Therefore, the reaction path and product selectivity can be optimized effectively by designing the hydrophilic and hydrophobic support.

In short, the physicochemical property of support for SACs operates the reaction activation and path from the long-range, which is different from single-site local coordination environment regulation. Facilitating reactant transfer and product desorption are common roles for catalyst design. In some cases, the rational design of pore structure can result confinement effect, eventually confining the electron structure of the metal site and reaction path. The SMSI effect can affect the electron structure of a single atom site thus operating the reaction performance. However, the characterization of SMSI is still not precise enough, and the identity of the contribution of the electron structure of the local coordination environment and SMSI in SACs still needs progress. In electrocatalyst design, the hydrophilic and hydrophobic support affect the side reaction rate, which should be considered.

5 Conclusions

In this review, we begin with a discussion of key points of single atom precise catalyze reaction process. We summarized three points that affect the reaction path in SAC, namely the unique electronic effect, geometry effect, and synergy effect in SAC. The narrow *d*-band electron structure and unique isolate atom site contribute to the activation and reaction path control, while the synergy between adjacent atom pairs contributes to the bond coupling and cleavage. In the actual catalytic process, these three effects both contribute to the catalytic process simultaneously sometimes. Hence, overall consideration of all aspects is important in the catalyst design and mechanism understanding.

Then, we elaborated recent progress of SACs in precise control reaction path of ECO_2RR, electrochemical synthesis urea, CO_2 hydrogenation, and CH_4 activation. SAC has been applied in numerous reactions, such as biomass conversion, fuel cells, advanced oxidation, and different kinds of selectivity hydrogenation reactions. Some of them show high TOF and high selectivity or specific reaction routes. Promoting the application of SAC toward more different reactions are thus important, which many bring out new reaction paths and new catalytic mechanism, and eventually guide catalyst design in a different field.

Finally, we emphasized the importance of support of a single atom site. Both morphology and structure of support affect the catalytic performance of single-atom sites. More importantly, the interaction between the single-atom site and support is important due to the electronic structure of single-atom site is defined by the support. Besides, the hydrophilic/hydrophobic of support is important in water solvent-involved reactions.

6 Prospects

6.1 Promote bond coupling on SACs

In this review, as we have discussed, SAC is good at the activation of reactants, such as activation of CO_2, and CH_4. The simple conversion of CO_2 or CH_4 on SAC always shows high product selectivity, such as ECO_2RR to CO on M-NC, and CH_4 selectivity oxidation to CH_3OH on metal oxide supported metal site. However, when the reaction refers to bond coupling, such as C–C or C–N bond coupling, the efficacy is limited. For instance, the C2 product selectivity of ECO_2RR is relatively low and few reports on SAC, the reaction process may happen on nanocatalyst while can happen on SAC. Therefore, deep investigation to explain and know the bond coupling mechanism is important. The final goal is to achieve a high selectivity bond coupling process of C–C and C–N bond coupling and extend to other types of bond coupling reactions. Besides, even though we did not discuss the bond cleavage process on SAC, it is important and always happens in many reactions, such as CH_3CH_2OH electrooxidation to CO_2 in direct ethanol fuel cell [51], in which the C–C bond cleavage is significant for the activity and energy efficiency improvement of the fuel cell. Therefore, rational design of the synergy multi-site to selective coupling or cleavage chemical bonds is important in further investigation.

6.2 The precise synthesis of SACs

In the design process of high-performance catalysis, the foundation is based on the structure design of the local environment and precise synthesis objective catalyst with a predicted coordination environment. Therefore, the development of precise synthesis methods for SACs is crucial. Typically, the synthesis methods of SACs can be categorized as (1) pyrolysis of carbon-rich precursors, such as MOFs, covalent organic frameworks, small organic molecules, polymers, and biomass; (2) physical and chemical deposition. For example, atomic layer deposition, chemical vapor deposition, and electrochemical deposition; (3) solution-phase synthesis; (4) ball milling; (5) electron/ion irradiation; (6) galvanic replacement reaction for synthesis SAA.

However, at present, SACs synthesized through these methods suffer from issues of uncontrolled coordination environments and lack of uniformity. For instance, single-atom Fe catalysts synthesized through pyrolysis exhibit four different site structures [128]. Although adjusting the precursor ratio can control the proportion of catalytic sites after pyrolysis, the resulting Fe catalysts still exhibit various states. This inconsistency in catalyst structure limited the reaction product selectivity and the mechanism investigation.

Recently, research on well-defined structures of molecular catalysis has garnered attention. For example, the CoPc molecular catalyst has been widely applied in the study of CO_2/CO reduction to produce CH_3OH. Utilizing its model-like structure, the mechanism of CO_2/CO competitive adsorption leading to CH_3OH production can be elucidated [129]. Hence, the development of a precise synthesis method of SAC is important for the depth understanding of the reaction mechanism.

6.3 Mechanism investigation

Beyond the high-density active sites, SACs present a notable advantage in their precisely defined site configurations, enabling the establishment of structure-function relationships. Recent years have witnessed a swift evolution in the theoretical understanding of catalysis, particularly driven by advancements in SAC research. The development of theory calculation has significantly refined catalyst design, simplifying the exploring processes of catalyst synthesis and performance screening. As we proceed into further development, the integration of insights into catalytic mechanisms offered by SACs with the power of *in situ* characterization and theory calculation holds the promise of expedient and rational design and synthesis of SACs.

6.3.1 *In situ* characterization development

During different catalytic reaction processes, numerous reaction intermediates are produced, and monitoring these intermediates is an essential step in exploring reaction mechanisms. Therefore, the development of various *in situ* dynamic characterization techniques for catalytic mechanism exploration is crucial. Techniques such as *in situ* infrared and *in situ* Raman spectroscopy can detect different reaction intermediates. Moreover, catalytic sites undergo dynamic changes during the reaction, posing a challenge for establishing structure-function relationships in catalytic mechanisms. Developing *in situ* characterization techniques to detect catalyst structural changes is therefore crucial. Techniques like *in situ* X-ray adsorption spectrum combined with *in situ* Raman spectroscopy can describe the conformational changes of SACs during the reaction process. Besides, Mössbauer spectroscopy is a characterization technique suitable for Fe/Sn-based catalysts. In our previous research, through *in situ* Mössbauer spectroscopy, dynamic changes in Sn single-atom sites during the reaction process could be clearly analyzed, getting information that other characterization techniques cannot provide. Therefore, the development of various combined *in situ* characterization techniques plays a crucial role in the further development of single-atom catalysis.

6.3.2 Developing theoretical calculation methodologies

In-depth research into reaction mechanisms necessitates not only the advancement of *in situ* characterization technologies but also the indispensable integration of theoretical calculations. The significance of theoretical calculations stems from the following reasons: elucidating prevailing experimental conclusions and summarizing reaction mechanisms as well as guiding catalyst designs. For instance, the performance of oxygen reduction reaction catalysts is intricately linked to the adsorption strength of metal sites to O intermediates. Despite the exceptional oxygen reduction reaction activity exhibited by Pt-based catalysts, their efficacy is limited by the high binding energy to O*. Therefore, by introducing heteroatoms such as Ni, Sn, Fe, and Pd through doping, the binding affinity of Pt sites to O atoms can be effectively decreased, consequently improving the oxygen reduction reaction performance. Summarizing research content and combining it with theory calculation affords an in-depth comprehension of the theoretical mechanism and structure-function relationship, facilitating purposeful catalyst design through combination with theoretical calculations. However, current theoretical calculations typically overlook environmental influences; for instance, electrocatalytic reactions often disregard the impact of electric fields and solvents during reactions. Thus, the development of novel calculation methodologies to accurately consider the catalytic environment may significantly enhance the investigation of catalytic mechanisms. Moreover, machine learning augments the improvement of mechanism investigation by swiftly screening existing data, distilling underlying structure-function relationships, and accurately predicting catalyst structures. This innovation markedly saves time and promotes catalyst development, significantly increasing efficiency. Consequently, the advancement of novel theoretical calculation methodologies and the cooperation of theory and experiment are of significance in the design and synthesis of SACs.

6.4 From laboratory to factory

Currently, most research related to SACs is in the basic research stage and is still relatively far from practical chemical engineering applications. In practical applications, although the micro-coordination environment of SAC metal sites can control catalytic efficiency and selectivity, the catalytic efficiency during the catalytic process is also influenced by mass transfer. Therefore, on the one hand, precise control should be exercised over the micro-coordination environment of SACs, and on the other hand, the morphology and types of supports should also be designed. Moreover, in the chemical synthesis process, the stability of the catalyst is tested more severely. The deactivation of a SAC may result from the destruction of local coordination or the reconstruction of support structures. Therefore, improving stability from the aspect of the local coordination environment and large-scale support is important. More importantly, the cost of a SAC in chemical synthesis is nonnegligible, so developing an inexpensive synthesis method for a SAC is important. In fundamental research, catalyst performance tests are always conducted under optimum test conditions. However, in the chemical synthesis process, the reaction conditions are also affected by the physical synthesis conditions. Improving the universality of the catalyst under different reaction conditions is an important aspect of its large-scale application. Additionally, the amount of catalyst used in industrial applications is substantial. The pollution and toxicity of the catalyst should be considered, and necessary protection should not be neglected. Furthermore, in actual reactions, numerous engineering problems are encountered, all of which need to be explored and researched in the next steps of the work (Fig. 13).

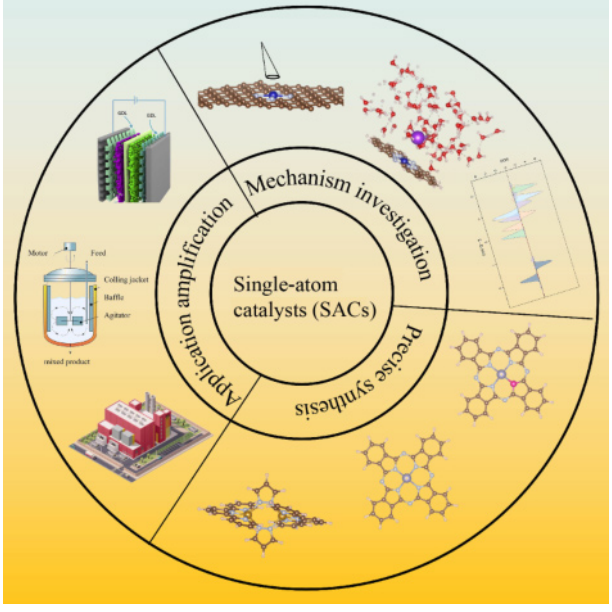

Fig. 13 Schematic perspective of synthesis, mechanism investigation, and applications amplification of SACs.

Competing interests The authors declare that they have no competing interests.

Acknowledgements This work was financially supported by the Strategic Priority Research Program of the Chinese Academy of Sciences (Grant No. XDB0600200), the National Key Research and Development Program of China (Grant No. 2021YFA1500502), the NSFC Center for Single-Atom Catalysis (Grant No. 22388102), the National Natural Science Foundation of China (Grant Nos. 22102176, U19A2015 and 21925803), CAS Project for Young Scientists in Basic Research (Grant Nos.YSBR-051, YSBR-022). The authors gratefully acknowledge the support of Photon Science Center for Carbon Neutrality.

References

1. Liu X, Dai L. Carbon-based metal-free catalysts. Nature Reviews. Materials, 2016, 1(11): 16064
2. Meirer F, Weckhuysen B M. Spatial and temporal exploration of heterogeneous catalysts with synchrotron radiation. Nature Reviews. Materials, 2018, 3(9): 324–340
3. Mitchell S, Pérez Ramírez J. Atomically precise control in the design of low-nuclearity supported metal catalysts. Nature Reviews. Materials, 2021, 6(11): 969–985
4. Zhao Z J, Liu S, Zha S, Cheng D, Studt F, Henkelman G, Gong J. Theory-guided design of catalytic materials using scaling relationships and reactivity descriptors. Nature Reviews. Materials, 2019, 4(12): 792–804
5. Suryanto B H R, Matuszek K, Choi J, Hodgetts R Y, Du H L, Bakker J M, Kang C S M, Cherepanov P V, Simonov A N, MacFarlane D R. Nitrogen reduction to ammonia at high efficiency and rates based on a phosphonium proton shuttle. Science, 2021, 372(6547): 1187–1191
6. Chen G F, Yuan Y, Jiang H, Ren S Y, Ding L X, Ma L, Wu T, Lu J, Wang H. Electrochemical reduction of nitrate to ammonia via direct eight-electron transfer using a copper-molecular solid catalyst. Nature Energy, 2020, 5(8): 605–613
7. Chang F, Tezsevin I, de Rijk J W, Meeldijk J D, Hofmann J P, Er S, Ngene P, de Jongh P E. Potassium hydride-intercalated graphite as an efficient heterogeneous catalyst for ammonia synthesis. Nature Catalysis, 2022, 5(3): 222–230
8. Pan X, Jiao F, Miao D, Bao X. Oxide-zeolite-based composite catalyst concept that enables syngas chemistry beyond Fischer-Tropsch synthesis. Chemical Reviews, 2021, 121(11): 6588–6609
9. Rahmati M, Safdari M S, Fletcher T H, Argyle M D, Bartholomew C H. Chemical and thermal sintering of supported metals with emphasis on cobalt catalysts during Fischer-Tropsch synthesis. Chemical Reviews, 2020, 120(10): 4455–4533
10. Rommens K T, Saeys M. Molecular views on Fischer-Tropsch synthesis. Chemical Reviews, 2023, 123(9): 5798–5858
11. Service R F. Lithium-ion battery development takes nobel. Science, 2019, 366(6463): 292
12. Degen F, Winter M, Bendig D, Tübke J. Energy consumption of current and future production of lithium-ion and post lithium-ion battery cells. Nature Energy, 2023, 8(11): 1284–1295
13. Gent W E, Busse G M, House K Z. The predicted persistence of cobalt in lithium-ion batteries. Nature Energy, 2022, 7(12): 1132–1143
14. Feng X, Ren D, He X, Ouyang M. Mitigating thermal runaway of lithium-ion batteries. Joule, 2020, 4(4): 743–770
15. Harper G, Sommerville R, Kendrick E, Driscoll L, Slater P, Stolkin R, Walton A, Christensen P, Heidrich O, Lambert S, et al. Recycling lithium-ion batteries from electric vehicles. Nature, 2019, 575(7781): 75–86
16. Chen L D. Cations play an essential role in CO_2 reduction. Nature Catalysis, 2021, 4(8): 641–642
17. Yan B, Li Y, Cao W, Zeng Z, Liu P, Ke Z, Yang G. Highly efficient and highly selective CO_2 reduction to CO driven by laser. Joule, 2022, 6(12): 2735–2744
18. Kang W, Lee C C, Jasniewski A J, Ribbe M W, Hu Y. Structural evidence for a dynamic metallocofactor during N_2 reduction by Mo-nitrogenase. Science, 2020, 368(6497): 1381–1385
19. Weliwatte N S, Minteer S D. Photo-bioelectrocatalytic CO_2 reduction for a circular energy landscape. Joule, 2021, 5(10): 2564–2592
20. Yu X, Han P, Wei Z, Huang L, Gu Z, Peng S, Ma J, Zheng G. Boron-doped graphene for electrocatalytic N_2 reduction. Joule, 2018, 2(8): 1610–1622
21. Qing G, Ghazfar R, Jackowski S T, Habibzadeh F, Ashtiani M M, Chen C P, Smith M R III, Hamann T W. Recent advances and challenges of electrocatalytic N_2 reduction to ammonia. Chemical Reviews, 2020, 120(12): 5437–5516
22. Tanifuji K, Ohki Y. Metal-sulfur compounds in N_2 reduction and nitrogenase-related chemistry. Chemical Reviews, 2020, 120(12): 5194–5251
23. Stephens I E L, Rossmeisl J, Chorkendorff I. Toward sustainable fuel cells. Science, 2016, 354(6318): 1378–1379
24. Gittleman C S, Jia H, De Castro E S, Chisholm C R I, Kim Y S. Proton conductors for heavy-duty vehicle fuel cells. Joule, 2021, 5(7): 1660–1677
25. Zhou Z, Zhang Y, Shen Y, Liu S, Zhang Y. Molecular engineering of polymeric carbon nitride: advancing applications from photocatalysis to biosensing and more. Chemical Society Reviews, 2018, 47(7): 2298–2321
26. Feng Y, Long S, Tang X, Sun Y, Luque R, Zeng X, Lin L. Earth-abundant 3d-transition-metal catalysts for lignocellulosic biomass conversion. Chemical Society Reviews, 2021, 50(10): 6042–6093
27. Sudarsanam P, Peeters E, Makshina E V, Parvulescu V I, Sels B F. Advances in porous and nanoscale catalysts for viable biomass conversion. Chemical Society Reviews, 2019, 48(8): 2366–2421
28. Fang R, Dhakshinamoorthy A, Li Y, Garcia H. Metal organic frameworks for biomass conversion. Chemical Society Reviews, 2020, 49(11): 3638–3687
29. Rimer J D. Rational design of zeolite catalysts. Nature Catalysis, 2018, 1(7): 488–489
30. Xu D, Zhang S N, Chen J S, Li X H. Design of the synergistic rectifying interfaces in Mott-Schottky catalysts. Chemical Reviews, 2023, 123(1): 1–30
31. Durand D J, Fey N. Computational ligand descriptors for catalyst design. Chemical Reviews, 2019, 119(11): 6561–6594
32. Motagamwala A H, Dumesic J A. Microkinetic modeling: a tool for rational catalyst design. Chemical Reviews, 2021, 121(2): 1049–1076
33. Su D, Lam Z, Wang Y, Han F, Zhang M, Liu B, Chen H. Ultralong durability of ethanol oxidation reaction via morphological design. Joule, 2023, 7(11): 2568–2582
34. Wang L, Meng S, Tang C, Zhan C, Geng S, Jiang K, Huang X, Bu L. PtNi/PtIn-skin fishbone-like nanowires boost alkaline hydrogen oxidation catalysis. ACS Nano, 2023, 17(18): 17779–17789
35. Mehmood R, Fan W, Hu X, Li J, Liu P, Zhang Y, Zhou Z, Wang J, Liu M, Zhang F. Confirming high-valent iron as highly active

species of water oxidation on the Fe, V-coupled bimetallic electrocatalyst: *in situ* analysis of X-ray absorption and mössbauer spectroscopy. Journal of the American Chemical Society, 2023, 145(22): 12206–12213

36. Das S, Pérez Ramírez J, Gong J, Dewangan N, Hidajat K, Gates B C, Kawi S. Core-shell structured catalysts for thermocatalytic, photocatalytic, and electrocatalytic conversion of CO_2. Chemical Society Reviews, 2020, 49(10): 2937–3004
37. Rideal E K. Prof. Paul Sabatier, For. Mem.R.S. Nature, 1941, 148(3750): 309
38. Tan T H, Xie B, Ng Y H, Abdullah S F B, Tang H Y M, Bedford N, Taylor R A, Aguey Zinsou K F, Amal R, Scott J. Unlocking the potential of the formate pathway in the photo-assisted sabatier reaction. Nature Catalysis, 2020, 3(12): 1034–1043
39. Hu S, Li W X. Sabatier principle of metal-support interaction for design of ultrastable metal nanocatalysts. Science, 2021, 374(6573): 1360–1365
40. Zhou Y, Wei F, Qi H, Chai Y, Cao L, Lin J, Wan Q, Liu X, Xing Y, Lin S, et al. Peripheral-nitrogen effects on the Ru_1 centre for highly efficient propane dehydrogenation. Nature Catalysis, 2022, 5(12): 1145–1156
41. Qiao B, Wang A, Yang X, Allard L F, Jiang Z, Cui Y, Liu J, Li J, Zhang T. Single-atom catalysis of CO oxidation using Pt_1/FeO_x. Nature Chemistry, 2011, 3(8): 634–641
42. Yang X F, Wang A, Qiao B, Li J, Liu J, Zhang T. Single-atom catalysts: a new frontier in heterogeneous catalysis. Accounts of Chemical Research, 2013, 46(8): 1740–1748
43. Liu L, Corma A. Metal catalysts for heterogeneous catalysis: from single atoms to nanoclusters and nanoparticles. Chemical Reviews, 2018, 118(10): 4981–5079
44. Zhang Y. Heterogeneous catalysis: single atoms on a roll. Nature Reviews Chemistry, 2018, 2(1): 0151
45. Wu X, Wang Q, Yang S, Zhang J, Cheng Y, Tang H, Ma L, Min X, Tang C, Jiang S P, et al. Sublayer-enhanced atomic sites of single atom catalysts through *in situ* atomization of metal oxide nanoparticles. Energy & Environmental Science, 2022, 15(3): 1183–1191
46. Jiang D, Wan G, Halldin Stenlid J, García Vargas C E, Zhang J, Sun C, Li J, Abild Pedersen F, Tassone C J, Wang Y. Dynamic and reversible transformations of subnanometre-sized palladium on ceria for efficient methane removal. Nature Catalysis, 2023, 6(7): 618–627
47. Agarwal N, Freakley S J, McVicker R U, Althahban S M, Dimitratos N, He Q, Morgan D J, Jenkins R L, Willock D J, Taylor S H, et al. Aqueous Au-Pd colloids catalyze selective CH_4 oxidation to CH_3OH with O_2 under mild conditions. Science, 2017, 358(6360): 223–227
48. Shoji S, Peng X, Yamaguchi A, Watanabe R, Fukuhara C, Cho Y, Yamamoto T, Matsumura S, Yu M W, Ishii S, et al. Photocatalytic uphill conversion of natural gas beyond the limitation of thermal reaction systems. Nature Catalysis, 2020, 3(2): 148–153
49. Xu S, Carter E A. Theoretical insights into heterogeneous (photo)electrochemical CO_2 reduction. Chemical Reviews, 2019, 119(11): 6631–6669
50. Rizo R, Arán Ais R M, Padgett E, Muller D A, Lázaro M J, Solla Gullón J, Feliu J M, Pastor E, Abruña H D. Pt-rich$_{core}$/Sn-rich$_{subsurface}$/Pt$_{skin}$ nanocubes as highly active and stable electrocatalysts for the ethanol oxidation reaction. Journal of the American Chemical Society, 2018, 140(10): 3791–3797
51. Yang X, Liang Z, Chen S, Ma M, Wang Q, Tong X, Zhang Q, Ye J, Gu L, Yang N. A phosphorus-doped Ag@Pd catalyst for enhanced C–C bond cleavage during ethanol electrooxidation. Small, 2020, 16(47): 2004727
52. Vijay S, Ju W, Brückner S, Tsang S C, Strasser P, Chan K. Unified mechanistic understanding of CO_2 reduction to CO on transition metal and single atom catalysts. Nature Catalysis, 2021, 4(12): 1024–1031
53. Tang Y, Li Y, Fung V, Jiang D E, Huang W, Zhang S, Iwasawa Y, Sakata T, Nguyen L, Zhang X, et al. Single rhodium atoms anchored in micropores for efficient transformation of methane under mild conditions. Nature Communications, 2018, 9(1): 1231
54. Xie P, Ding J, Yao Z, Pu T, Zhang P, Huang Z, Wang C, Zhang J, Zecher Freeman N, Zong H, et al. Oxo dicopper anchored on carbon nitride for selective oxidation of methane. Nature Communications, 2022, 13(1): 1375
55. Wang Z, Liu S, Zhao X, Wang M, Zhang L, Qian T, Xiong J, Yang C, Yan C. Interfacial defect engineering triggered by single atom doping for highly efficient electrocatalytic nitrate reduction to ammonia. ACS Materials Letters, 2023, 5(4): 1018–1026
56. Ding J, Teng Z, Su X, Kato K, Liu Y, Xiao T, Liu W, Liu L, Zhang Q, Ren X, et al. Asymmetrically coordinated cobalt single atom on carbon nitride for highly selective photocatalytic oxidation of CH_4 to CH_3OH. Chem, 2023, 9(4): 1017–1035
57. Ding J, Wei Z, Li F, Zhang J, Zhang Q, Zhou J, Wang W, Liu Y, Zhang Z, Su X, et al. Atomic high-spin cobalt(II) center for highly selective electrochemical CO reduction to CH_3OH. Nature Communications, 2023, 14(1): 6550
58. Wang Q, Wang H, Cao H, Tung C W, Liu W, Hung S F, Wang W, Zhu C, Zhang Z, Cai W, et al. Atomic metal-non-metal catalytic pair drives efficient hydrogen oxidation catalysis in fuel cells. Nature Catalysis, 2023, 6(10): 916–926
59. Wang Y, Mao J, Meng X, Yu L, Deng D, Bao X. Catalysis with two-dimensional materials confining single atoms: concept, design, and applications. Chemical Reviews, 2019, 119(3): 1806–1854
60. Nørskov J K, Stoltze P. Theoretical aspects of surface reactions. Surface Science, 1987, 189–190: 91–105
61. Greiner M T, Jones T E, Beeg S, Zwiener L, Scherzer M, Girgsdies F, Piccinin S, Armbrüster M, Knop Gericke A, Schlögl R. Free-atom-like d states in single-atom alloy catalysts. Nature Chemistry, 2018, 10(10): 1008–1015
62. Rosen A S, Vijay S, Persson K A. Free-atom-like d states beyond the dilute limit of single-atom alloys. Chemical Science, 2023, 14(6): 1503–1511
63. Spivey T D, Holewinski A. Selective interactions between free-atom-like d-states in single-atom alloy catalysts and near-frontier molecular orbitals. Journal of the American Chemical Society, 2021, 143(31): 11897–11902

64. Darby M T, Réocreux R, Sykes E C H, Michaelides A, Stamatakis M. Elucidating the stability and reactivity of surface intermediates on single-atom alloy catalysts. ACS Catalysis, 2018, 8(6): 5038–5050
65. Yu S, Cheng X, Wang Y, Xiao B, Xing Y, Ren J, Lu Y, Li H, Zhuang C, Chen G. High activity and selectivity of single palladium atom for oxygen hydrogenation to H_2O_2. Nature Communications, 2022, 13(1): 4737
66. Li W, Wu G, Hu W, Dang J, Wang C, Weng X, da Silva I, Manuel P, Yang S, Guan N, et al. Direct propylene epoxidation with molecular oxygen over cobalt-containing zeolites. Journal of the American Chemical Society, 2022, 144(9): 4260–4268
67. Qiao B, Liu J, Wang Y G, Lin Q, Liu X, Wang A, Li J, Zhang T, Liu J. Highly efficient catalysis of preferential oxidation of CO in H_2-rich stream by gold single-atom catalysts. ACS Catalysis, 2015, 5(11): 6249–6254
68. Ma W, Mao J, He C T, Shao L, Liu J, Wang M, Yu P, Mao L. Highly selective generation of singlet oxygen from dioxygen with atomically dispersed catalysts. Chemical Science (Cambridge), 2022, 13(19): 5606–5615
69. Shang Q, Tang N, Qi H, Chen S, Xu G, Wu C, Pan X, Wang X, Cong Y. Cong Y. A palladium single-atom catalyst toward efficient activation of molecular oxygen for cinnamyl alcohol oxidation. Chinese Journal of Catalysis, 2020, 41(12): 1812–1817
70. Li Z, Chen Y, Ji S, Tang Y, Chen W, Li A, Zhao J, Xiong Y, Wu Y, Gong Y, et al. Iridium single-atom catalyst on nitrogen-doped carbon for formic acid oxidation synthesized using a general host-guest strategy. Nature Chemistry, 2020, 12(8): 764–772
71. Xiong Y, Dong J, Huang Z Q, Xin P, Chen W, Wang Y, Li Z, Jin Z, Xing W, Zhuang Z, et al. Single-atom Rh/N-doped carbon electrocatalyst for formic acid oxidation. Nature Nanotechnology, 2020, 15(5): 390–397
72. Li W, Madan S E, Réocreux R, Stamatakis M. Elucidating the reactivity of oxygenates on single-atom alloy catalysts. ACS Catalysis, 2023, 13(24): 15851–15868
73. Ni W, Meibom J L, Hassan N U, Chang M, Chu Y C, Krammer A, Sun S, Zheng Y, Bai L, Ma W, et al. Synergistic interactions between PtRu catalyst and nitrogen-doped carbon support boost hydrogen oxidation. Nature Catalysis, 2023, 6(9): 773–783
74. Meng G, Lan W, Zhang L, Wang S, Zhang T, Zhang S, Xu M, Wang Y, Zhang J, Yue F, et al. Synergy of single atoms and lewis acid sites for efficient and selective lignin disassembly into monolignol derivatives. Journal of the American Chemical Society, 2023, 145(23): 12884–12893
75. Dong C, Gao Z, Li Y, Peng M, Wang M, Xu Y, Li C, Xu M, Deng Y, Qin X, et al. Fully exposed palladium cluster catalysts enable hydrogen production from nitrogen heterocycles. Nature Catalysis, 2022, 5(6): 485–493
76. Fu N, Liang X, Wang X, Gan T, Ye C, Li Z, Liu J C, Li Y. Controllable conversion of platinum nanoparticles to single atoms in Pt/CeO_2 by laser ablation for efficient CO oxidation. Journal of the American Chemical Society, 2023, 145(17): 9540–9547
77. Fang Y, Zhang Q, Zhang H, Li X, Chen W, Xu J, Shen H, Yang J, Pan C, Zhu Y, et al. Dual activation of molecular oxygen and surface lattice oxygen in single atom Cu_1/TiO_2 catalyst for CO oxidation. Angewandte Chemie International Edition, 2022, 61(48): e202212273
78. Niu H, Zhang Z, Wang X, Wan X, Shao C, Guo Y. Theoretical insights into the mechanism of selective nitrate-to-ammonia electroreduction on single-atom catalysts. Advanced Functional Materials, 2021, 31(11): 2008533
79. Leverett J, Tran Phu T, Yuwono J A, Kumar P, Kim C, Zhai Q, Han C, Qu J, Cairney J, Simonov A N, et al. Tuning the coordination structure of Cu-N-C single atom catalysts for simultaneous electrochemical reduction of CO_2 and NO_3^- to urea. Advanced Energy Materials, 2022, 12(32): 2201500
80. Yang W, Polo Garzon F, Zhou H, Huang Z, Chi M, Meyer H III, Yu X, Li Y, Wu Z. Boosting the activity of Pd single atoms by tuning their local environment on ceria for methane combustion. Angewandte Chemie International Edition, 2023, 62(5): e202217323
81. Jia G, Sun M, Wang Y, Shi Y, Zhang L, Cui X, Huang B, Yu J C. Asymmetric coupled dual-atom sites for selective photoreduction of carbon dioxide to acetic acid. Advanced Functional Materials, 2022, 32(41): 2206817
82. Chu C, Huang D, Gupta S, Weon S, Niu J, Stavitski E, Muhich C, Kim J H. Neighboring Pd single atoms surpass isolated single atoms for selective hydrodehalogenation catalysis. Nature Communications, 2021, 12(1): 5179
83. Liu P, Huang X, Mance D, Copéret C. Atomically dispersed iridium on MgO(111) nanosheets catalyses benzene-ethylene coupling towards styrene. Nature Catalysis, 2021, 4(11): 968–975
84. Ro I, Qi J, Lee S, Xu M, Yan X, Xie Z, Zakem G, Morales A, Chen J G, Pan X, et al. Bifunctional hydroformylation on heterogeneous Rh-WO_x pair site catalysts. Nature, 2022, 609(7926): 287–292
85. Liu W, Feng H, Yang Y, Niu Y, Wang L, Yin P, Hong S, Zhang B, Zhang X, Wei M. Highly-efficient RuNi single-atom alloy catalysts toward chemoselective hydrogenation of nitroarenes. Nature Communications, 2022, 13(1): 3188
86. Cao H, Zhang Z, Chen J W, Wang Y G. Potential-dependent free energy relationship in interpreting the electrochemical performance of CO_2 reduction on single atom catalysts. ACS Catalysis, 2022, 12(11): 6606–6617
87. Li J, Zeng H, Dong X, Ding Y, Hu S, Zhang R, Dai Y, Cui P, Xiao Z, Zhao D, et al. Selective CO_2 electrolysis to CO using isolated antimony alloyed copper. Nature Communications, 2023, 14(1): 340
88. Zhang M, Zhang Z, Zhao Z, Huang H, Anjum D H, Wang D, He J, Huang K W. He J h, Huang K W. Tunable selectivity for electrochemical CO_2 reduction by bimetallic Cu-Sn catalysts: elucidating the roles of Cu and Sn. ACS Catalysis, 2021, 11(17): 11103–11108
89. Yang H B, Hung S F, Liu S, Yuan K, Miao S, Zhang L, Huang X, Wang H Y, Cai W, Chen R, et al. Atomically dispersed Ni(I) as the active site for electrochemical CO_2 reduction. Nature Energy, 2018, 3(2): 140–147
90. Deng Y, Zhao J, Wang S, Chen R, Ding J, Tsai H J, Zeng W J,

Hung S F, Xu W, Wang J, et al. Operando spectroscopic analysis of axial oxygen-coordinated single-Sn-atom sites for electrochemical CO_2 reduction. Journal of the American Chemical Society, 2023, 145(13): 7242–7251

91. Ding J, Bin Yang H, Ma X L, Liu S, Liu W, Mao Q, Huang Y, Li J, Zhang T, Liu B. A tin-based tandem electrocatalyst for CO_2 reduction to ethanol with 80% selectivity. Nature Energy, 2023, 8(12): 1386–1394
92. Zheng X, De Luna P, García de Arquer F P, Zhang B, Becknell N, Ross M B, Li Y, Banis M N, Li Y, Liu M, et al. Sulfur-modulated tin sites enable highly selective electrochemical reduction of CO_2 to formate. Joule, 2017, 1(4): 794–805
93. Li W, Li L, Xia Q, Hong S, Wang L, Yao Z, Wu T S, Soo Y L, Zhang H, Lo T W B, et al. Lowering C–C coupling barriers for efficient electrochemical CO_2 reduction to C_2H_4 by jointly engineering single Bi atoms and oxygen vacancies on CuO. Applied Catalysis B: Environmental, 2022, 318: 121823
94. Cao Y, Chen S, Bo S, Fan W, Li J, Jia C, Zhou Z, Liu Q, Zheng L, Zhang F. Single atom Bi decorated copper alloy enables C–C coupling for electrocatalytic reduction of CO_2 into C_{2+} products**. Angewandte Chemie International Edition, 2023, 62(30): e202303048
95. Jiang M, Zhu M, Wang M, He Y, Luo X, Wu C, Zhang L, Jin Z. Review on electrocatalytic coreduction of carbon dioxide and nitrogenous species for urea synthesis. ACS Nano, 2023, 17(4): 3209–3224
96. Zhang X, Zhu X, Bo S, Chen C, Qiu M, Wei X, He N, Xie C, Chen W, Zheng J, et al. Identifying and tailoring C–N coupling site for efficient urea synthesis over diatomic Fe-Ni catalyst. Nature Communications, 2022, 13(1): 5337
97. Liu Y, Tu X, Wei X, Wang D, Zhang X, Chen W, Chen C, Wang S. C-bound or O-bound surface: which one boosts electrocatalytic urea synthesis? Angewandte Chemie International Edition, 2023, 62(19): e202300387
98. Li J, Zhang Y, Kuruvinashetti K, Kornienko N. Construction of C–N bonds from small-molecule precursors through heterogeneous electrocatalysis. Nature Reviews. Chemistry, 2022, 6(5): 303–319
99. Liu J, Smith S C, Gu Y, Kou L. C–N coupling enabled by N–N bond breaking for electrochemical urea production. Advanced Functional Materials, 2023, 33(47): 2305894
100. Zhang X, Zhu X, Bo S, Chen C, Cheng K, Zheng J, Li S, Tu X, Chen W, Xie C, et al. Electrocatalytic urea synthesis with 63.5% faradaic efficiency and 100% N-selectivity via one-step C–N coupling. Angewandte Chemie International Edition, 2023, 62(33): e202305447
101. Chen L, Allec S I, Nguyen M T, Kovarik L, Hoffman A S, Hong J, Meira D, Shi H, Bare S R, Glezakou V A, et al. Dynamic evolution of palladium single atoms on anatase titania support determines the reverse water-gas shift activity. Journal of the American Chemical Society, 2023, 145(19): 10847–10860
102. Millet M M, Algara Siller G, Wrabetz S, Mazheika A, Girgsdies F, Teschner D, Seitz F, Tarasov A, Levchenko S V, Schlögl R, et al. Ni single atom catalysts for CO_2 activation. Journal of the American Chemical Society, 2019, 141(6): 2451–2461
103. Du P, Qi R, Zhang Y, Gu Q, Xu X, Tan Y, Liu X, Wang A, Zhu B, Yang B, et al. Single-atom-driven dynamic carburization over Pd_1-FeO_x catalyst boosting CO_2 conversion. Chem, 2022, 8(12): 3252–3262
104. Yang B, Wang Y, Gao B, Zhang L, Guo L. Size-dependent active site and its catalytic mechanism for CO_2 hydrogenation reactivity and selectivity over Re/TiO_2. ACS Catalysis, 2023, 13(15): 10364–10374
105. Wang D, Yuan Z, Wu X, Xiong W, Ding J, Zhang Z, Huang W. Ni single atoms confined in nitrogen-doped carbon nanotubes for active and selective hydrogenation of CO_2 to CO. ACS Catalysis, 2023, 13(10): 7132–7138
106. Shao X, Yang X, Xu J, Liu S, Miao S, Liu X, Su X, Duan H, Huang Y, Zhang T. Iridium single-atom catalyst performing a quasi-homogeneous hydrogenation transformation of CO_2 to formate. Chem, 2019, 5(3): 693–705
107. Yang T, Mao X, Zhang Y, Wu X, Wang L, Chu M, Pao C W, Yang S, Xu Y, Huang X. Coordination tailoring of Cu single sites on C_3N_4 realizes selective CO_2 hydrogenation at low temperature. Nature Communications, 2021, 12(1): 6022
108. Chen Y, Li H, Zhao W, Zhang W, Li J, Li W, Zheng X, Yan W, Zhang W, Zhu J, et al. Optimizing reaction paths for methanol synthesis from CO_2 hydrogenation via metal-ligand cooperativity. Nature Communications, 2019, 10(1): 1885
109. Ye X, Yang C, Pan X, Ma J, Zhang Y, Ren Y, Liu X, Li L, Huang Y. Highly selective hydrogenation of CO_2 to ethanol via designed bifunctional Ir_1-In_2O_3 single-atom catalyst. Journal of the American Chemical Society, 2020, 142(45): 19001–19005
110. Zheng K, Li Y, Liu B, Jiang F, Xu Y, Liu X. Ti-doped CeO_2 stabilized single-atom rhodium catalyst for selective and stable CO_2 hydrogenation to ethanol. Angewandte Chemie International Edition, 2022, 61(44): e202210991
111. Gani T Z H, Kulik H J. Understanding and breaking scaling relations in single-site catalysis: methane to methanol conversion by Fe(IV)=O. ACS Catalysis, 2018, 8(2): 975–986
112. Schwach P, Pan X, Bao X. Direct conversion of methane to value-added chemicals over heterogeneous catalysts: challenges and prospects. Chemical Reviews, 2017, 117(13): 8497–8520
113. Tang X, Wang L, Yang B, Fei C, Yao T, Liu W, Lou Y, Dai Q, Cai Y, Cao X M, et al. Direct oxidation of methane to oxygenates on supported single Cu atom catalyst. Applied Catalysis B: Environmental, 2021, 285: 119827
114. Yang J, Huang Y, Qi H, Zeng C, Jiang Q, Cui Y, Su Y, Du X, Pan X, Liu X, et al. Modulating the strong metal-support interactian of single-atom catalysts via vicinal structure decoration. Nature Communications, 2022, 13(1): 4244
115. Fang G, Wei F, Lin J, Zhou Y, Sun L, Shang X, Lin S, Wang X. Retrofitting Zr-Oxo nodes of UiO-66 by Ru single atoms to boost methane hydroxylation with nearly total selectivity. Journal of the American Chemical Society, 2023, 145(24): 13169–13180
116. Grundner S, Markovits M A C, Li G, Tromp M, Pidko E A, Hensen E J M, Jentys A, Sanchez Sanchez M, Lercher J A. Single-site trinuclear copper oxygen clusters in mordenite for selective conversion of methane to methanol. Nature Communications, 2015, 6(1): 7546
117. Yu B, Cheng L, Dai S, Jiang Y, Yang B, Li H, Zhao Y, Xu J,

Zhang Y, Pan C, et al. Silver and copper dual single atoms boosting direct oxidation of methane to methanol via synergistic catalysis. Advanced Science, 2023, 10(26): 2302143

118. Shen X, Wu D, Fu X Z, Luo J L. Highly selective conversion of methane to ethanol over $CuFe_2O_4$-carbon nanotube catalysts at low temperature. Chinese Chemical Letters, 2022, 33(1): 390–393
119. Wang Z, Liu Y, Zhang H, Zhou X. Cubic platinum nanoparticles capped with Cs_2[closo-$B_{12}H_{12}$] as an effective oxidation catalyst for converting methane to ethanol. Journal of Colloid and Interface Science, 2020, 566: 135–142
120. Zhou Y, Zhang L, Wang W. Direct functionalization of methane into ethanol over copper modified polymeric carbon nitride via photocatalysis. Nature Communications, 2019, 10(1): 506
121. Su J, Musgrave C B III, Song Y, Huang L, Liu Y, Li G, Xin Y, Xiong P, Li M M J, Wu H, et al. Strain enhances the activity of molecular electrocatalysts via carbon nanotube supports. Nature Catalysis, 2023, 6(9): 818–828
122. Zhou S, Ma W, Anjum U, Kosari M, Xi S, Kozlov S M, Zeng H C. Strained few-layer MoS_2 with atomic copper and selectively exposed in-plane sulfur vacancies for CO_2 hydrogenation to methanol. Nature Communications, 2023, 14(1): 5872
123. Shamzhy M, Opanasenko M, Concepción P, Martínez A. New trends in tailoring active sites in zeolite-based catalysts. Chemical Society Reviews, 2019, 48(4): 1095–1149
124. Deng X, Qin B, Liu R, Qin X, Dai W, Wu G, Guan N, Ma D, Li L. Zeolite-eencaged isolated platinum ions enable heterolytic dihydrogen activation and selective hydrogenations. Journal of the American Chemical Society, 2021, 143(49): 20898–20906
125. Han B, Guo Y, Huang Y, Xi W, Xu J, Luo J, Qi H, Ren Y, Liu X, Qiao B, et al. Strong metal-support interactions between Pt single atoms and TiO_2. Angewandte Chemie International Edition, 2020, 59(29): 11824–11829
126. Yang J, Li W, Wang D, Li Y. Electronic metal-support interaction of single-atom catalysts and applications in electrocatalysis. Advanced Materials, 2020, 32(49): 2003300
127. Wakerley D, Lamaison S, Ozanam F, Menguy N, Mercier D, Marcus P, Fontecave M, Mougel V. Bio-inspired hydrophobicity promotes CO_2 reduction on a Cu surface. Nature Materials, 2019, 18(11): 1222–1227
128. Li X, Cao C S, Hung S F, Lu Y R, Cai W, Rykov A I, Miao S, Xi S, Yang H, Hu Z, et al. Identification of the electronic and structural dynamics of catalytic centers in single-Fe-atom material. Chem, 2020, 6(12): 3440–3454
129. Ren X, Zhao J, Li X, Shao J, Pan B, Salamé A, Boutin E, Groizard T, Wang S, Ding J, et al. *In-situ* spectroscopic probe of the intrinsic structure feature of single-atom center in electrochemical CO/CO_2 reduction to methanol. Nature Communications, 2023, 14(1): 3401